J. Fluid Mech. (2005), *vol.* 530, *pp.* 1–30.
doi:10.1017/S0022112004003234 Printed in the United Kingdom

The structure and evolution of elliptical barotropic modons

By R. KHVOLES[1], D. BERSON[2] AND Z. KIZNER[1,2,†]

[1]Department of Mathematics Bar-Ilan University, Ramat-Gan 52900, Israel

[2]Department of Physics Bar-Ilan University, Ramat-Gan 52900, Israel

(Received 30 September 2003 and in revised form 6 November 2004)

Explicit stationary solutions to the equations of vorticity conservation on the f- and β-planes are considered, describing barotropic dipoles (modons) with elliptical frontiers. The far field – outside the elliptical separatrix demarcating the regions of closed and open streamlines – is given analytically, whereas the interior is solved numerically using a successive linearization algorithm. Both ellipses extended along the translation axis and those extended in the transverse direction are considered. In the latter case, it is shown that, among the possible solutions, there exist the so-called supersmooth modons marked by continuity of the vorticity derivatives at the separatrix. On the β-plane, the separatrix aspect ratio that allows a supersmooth solution varies depending on the modon translation speed and size, while on the f-plane, there is only one such separatrix aspect ratio. In this context, the limiting transition from the β-plane to the f-plane is discussed. The dependence between the absolute (or relative) vorticity q and the 'co-moving' streamfunction Ψ, which is nonlinear in the interior of non-circular modons, is analysed in detail for both β- and f-planes, the main concern being the relation between the separatrix form, on the one hand, and the shape of the q against Ψ scattergraph on the other. The stability of elliptical dipoles versus the separatrix aspect ratio is examined based on numerical simulations of the temporal evolution of the modons found. The supersmooth modons appear to be the most stable among all the elliptical dipoles.

1. Introduction

The first dipole vortex solution was suggested independently by Lamb (1895, 1906) and Chaplygin (1903) (see the historical essay of Meleshko & van Heijst 1994). This is the well-known translating circular dipole solution to the Euler equations in two dimensions (valid on the f-plane). On the β-plane, an analogous circular translating dipole solution was constructed by Larichev & Reznik (1976), whereas a standing circular β-plane dipole was found by Stern (1975), who suggested the term 'modon' to designate such vortices. Since that time, this term has been loosely used when speaking of stationary barotropic and baroclinic vortex pairs or similar configurations. A characteristic property of the translating barotropic dipoles (whether on the f- or β-plane) is the continuity of their vorticity fields. In contrast, the vorticity field of the standing Stern modon is discontinuous. Recent investigations suggest that the

† Author to whom correspondence should be addressed: zinovyk@mail.biu.ac.il.

continuity of vorticity is vital for the stability of vortices (Paldor 1999; Kizner & Berson 2000; Kizner, Berson & Khvoles 2003).

In steadily translating localized β-plane dipoles, when considered in a co-moving coordinate frame, a closed contour (separatrix) Γ exists which demarcates the interior (or core) region, where the streamlines are closed, from the exterior (or far-field) region, where the streamlines are open. The term 'localized' is used to distinguish the solutions possessing finite kinetic momentum, energy etc. and thus characterized by sufficiently fast decrease of the flow at infinity, i.e. when the distance from the vortex core increases. Clearly, owing to the stationarity, the contours of constant absolute vorticity q coincide with the streamlines – the contours of constant 'co-moving streamfunction' Ψ, meaning that there is a functional dependence between q and Ψ. This dependence is linear in the far-field of a β-plane modon; in its f-plane counterpart, the exterior vorticity is zero (note that on the f-plane, q signifies just the relative vorticity since here $\beta = 0$), whereas in a standing β-plane vortex the exterior streamfunction is zero. Regarding the q *vs.* Ψ relation in the interior domain, although it is linear in the classical modons of Lamb, Stern and Larichev & Reznik (1983), generally, it can be nonlinear (see the references below).

In this paper we focus on the barotropic 'nonlinear' modons – those whose q *vs.* Ψ dependences in the interior domain are nonlinear – accepting the broad interpretation of the term 'modon', but restricting it to form-preserving steadily translating or standing vortex pairs that possess a separatix. In this sense, e.g. the Lamb, Stern and Larichev–Reznik dipoles are modons, whereas the shielded nonlinear standing f-plane dipole solution suggested by Hesthaven *et al.* (1995) is not.

Although, Hesthaven *et al.* (1995) showed numerically the essential instability of their standing dipole, they observed that such a vortex transforms into a stable quasi-stationary translating modon. The separatrix of the emerged translating modon had a quasi-elliptical shape extended in the direction perpendicular to the translation axis, and the q *vs.* Ψ scattergraph in the interior had a clearly nonlinear shape. The standing modon of Stern was also found to be unstable (Kizner & Berson 2000) since small perturbations with westward net impulse led to a fast disintegration of the vortex pair, whereas those with eastward net impulse resulted in the modon's mild transitions to slowly translating dipoles of the Larichev–Reznik type. It is not inconceivable that instability is a common property of all standing dipoles, because to balance the self-propulsion natural in vortex pairs, such a dipole must possess some peculiar qualities. These are, e.g., the unlimited (on the right-hand and left-hand sides of the translation axis) areas of oppositely signed vorticity enclosing the dipole proper to the solution of Hesthaven *et al.* and the vorticity jump across the separatrix in the Stern modon. Thus, it comes as no surprise that the emergence of standing dipoles was never observed in numerical or laboratory experiments.

In contrast, the emergence of nonlinear translating modons was reported in a number of publications devoted to numerical simulations of the temporal evolution and interaction of vortices, and in most of them the nonlinearity of the q *vs.* Ψ relation in the interior was evidenced. For example, in an experiment conducted by McWilliams & Zabusky (1982), two merging Larichev–Reznik dipoles created a quasi-stationary vortex with a nonlinear interior dependence of q upon Ψ clearly visible in the q *vs.* Ψ scattergraph; a similar result was obtained by McWilliams (1983) who studied the modon generation by monopole collision (inviscid model) and by Nielsen & Juul Rasmussen (1997) who followed the viscid evolution of a Lamb modon. With these studies ranks that of Hesthaven *et al.* cited above. The emergence of steadily translating nonlinear modon-like structures was observed also in baroclinic

models on the β-plane – first by Morrel & McWilliams (1997) in their numerical experiments with high vertical resolution and later in our two-layer experiments with exact baroclinic modon solutions (Kizner, Berson & Khvoles 2002). All these results point to the importance of the search for explicit nonlinear modon solutions.

Weakly nonlinear dipolar structures studied by Nycander (1988) with the use of asymptotic methods displayed slight quasi-elliptical extension of the vortex separatrix. Strongly elliptical translating modons were considered by Boyd & Ma (1990) who suggested a numerical method for the construction of such f-plane vortices. They, however, considered only the dipoles extended in the direction of the modon translation (that were never observed in numerical or in laboratory experiments) and revealed the specific nonlinear internal q *vs.* Ψ dependence characteristic of such ellipses.

To the best of our knowledge, Nycander and Boyd & Ma were the first to indicate the existence of dependence between the separatrix shape, on the one hand, and the interior q *vs.* Ψ relation, on the other. Prescribing the modon shape (eccentricity), Boyd & Ma analysed the resulting q *vs.* Ψ scattergraphs. Approaches conceptually opposite to that of Boyd & Ma were employed by Nycander (1988) in his work devoted to β-plane vortices and by Verkley (1993), who constructed weakly nonlinear barotropic form-preserving solutions on a sphere.

In our recent study (Kizner *et al.* 2003), a method for the construction of stationary non-circular (and hence, nonlinear) two-layer β-plane modon solutions was suggested and applied, numerous baroclinic elliptical modons being studied. The circularity and linearity were shown to be equivalent characteristics of the modon. Clearly, this conclusion is valid for both baroclinic and barotropic modons.

Methodologically, the search for nonlinear modons is facilitated by the existence of a separatrix, which allows a separate (in some sense) construction of the interior and exterior solutions with their matching. The far field is determined analytically, while the interior is solved numerically with the use of a Newton–Kantorovich algorithm and a collocation method combined with polynomial approximation of the solution sought. In this paper, we use a particular case of this approach to construct barotropic nonlinear modon solutions on the f- and β-planes. The main objective of this paper is the exploration of the properties of elliptical barotropic modons on the f-plane (translating modons only) and on the β-plane (translating and standing modons). We consider only dipolar modons based on the fact that conventional multipolar translating and standing modons (i.e. those corresponding to the second, third, etc. branches of the dispersion relations of the Lamb, Stern and Larichev–Reznik solutions) are strongly unstable (Orlandi, Verzicco & van Heijst 1994; Kizner & Berson 2000).

In § 2, the mathematical set-up of the problem is given and the numerical method used is described. The elliptical modon solutions found are presented and classified in § 3; here, the dependence between the internal q *vs.* Ψ relations and the modon parameters is established, and the existence of supersmooth modons is shown (§§ 3.1.2 and 3.2). In § 4, the stability of elliptical modons is examined in a series of numerical experiments, and remarkable persistence of the supersmooth modons is shown.

2. Problem and method

2.1. *Formulation*

Consider a stationary solution that describes a non-divergent barotropic dipole vortex translating with a constant speed U in a fluid layer of constant thickness. For such

solutions, the vorticity conservation in the co-moving frame of coordinates is given by the equation

$$J(\Psi, q) = 0. \tag{1}$$

Here, $\Psi = \psi + Uy$ is the 'co-moving streamfunction', ψ is the streamfunction defined via the relationships $u = -\partial\psi/\partial y$, $v = \partial\psi/\partial x$ (where u and v are the velocity components in the non-moving frame); q is the conserved vorticity: $q = \Delta\psi + \beta y$ in the β-plane case (absolute vorticity) and $q = \Delta\psi$ in the f-plane case; $J(\ ,\ )$ and Δ are the Jacobian and Laplacian operators, respectively; x and y are Cartesian coordinates in the frame attached to the dipole, the vortex is assumed to translate in the x-direction. On the f-plane, a localized non-divergent steady-state dipole can move in any direction, while on the β-plane only the eastward translation is permitted (Larichev & Reznik 1976). Thus, for the β-plane, we choose x to be eastward, y northward and $U \geqslant 0$. The solution sought is assumed antisymmetrical about the x-axis and symmetrical about the y-axis (in the co-moving coordinate system).

Because of the above symmetry/antisymmetry restriction, the modon separatrix Γ (see § 1) is symmetrical about both axes, and Ψ and q assume zero values at Γ. We will confine ourselves to elliptical separatrices only.

In f-plane modons, the streamfunction of the exterior flow, $\psi^{(Ex)}$, is taken as a harmonic function, i.e.

$$\Delta\psi^{(Ex)} = 0, \tag{2}$$

while in translating β-plane modons, it satisfies the Helmholtz equation

$$\Delta\psi^{(Ex)} = l^2\psi^{(Ex)}, \quad l^2 = \beta/U, \tag{3}$$

where $U > 0$; in a standing β-plane modon $\psi^{(Ex)} = 0$ (Stern 1975). It is seen that in all these cases, $\psi^{(Ex)}$ satisfies (1). In the general case of a non-circular modon, the streamfunction of the interior flow, $\psi^{(In)}$, satisfies the nonlinear equation

$$J\left(\Psi^{(In)}, q^{(In)}\right) = 0. \tag{4}$$

In addition, we require continuity of the streamfunction and velocity fields at the separatrix Γ, so that the boundary conditions at Γ are

$$\Psi^{(In)}\big|_\Gamma = \Psi^{(Ex)}\big|_\Gamma = 0, \quad \left.\frac{\partial}{\partial n}\Psi^{(In)}\right|_\Gamma = \left.\frac{\partial}{\partial n}\Psi^{(Ex)}\right|_\Gamma, \tag{5}$$

where n is the (external) normal to the contour Γ. Note that, in translating modons, fulfilling (4) and (5) guarantees that $q^{(In)}|_\Gamma = q^{(Ex)}|_\Gamma = 0$ (Kizner *et al.* 2003).

2.2. *Exterior flow*

On the f-plane, the exterior flow in a co-moving frame of reference can be thought of as uniform at infinity ($x \to \pm\infty$) potential flow rounding an elliptical obstacle (see (2)). The corresponding solution is unique; it is described by Lamb (1932), for example. In the Cartesian coordinates x and y, this solution is given by the formulae

$$\psi^{(Ex)} = -Uy\frac{r_y}{r_y - r_x}\left(1 - \sqrt{\frac{x^2 + y^2 - c^2 + \sqrt{(x^2 + y^2 + c^2)^2 - 4y^2c^2}}{x^2 + y^2 + c^2 + \sqrt{(x^2 + y^2 + c^2)^2 - 4y^2c^2}}}\right), \quad \varepsilon \geqslant 1, \tag{6a}$$

$$\psi^{(Ex)} = Uy\frac{r_y}{r_x - r_y}\left(1 - \sqrt{\frac{x^2 + y^2 + c^2 + \sqrt{(x^2 + y^2 + c^2)^2 - 4x^2c^2}}{x^2 + y^2 - c^2 + \sqrt{(x^2 + y^2 + c^2)^2 - 4x^2c^2}}}\right), \quad \varepsilon < 1. \tag{6b}$$

where $c = \sqrt{|r_x^2 - r_y^2|}$; r_x and r_y are the ellipse radii in the x- and y-directions, respectively; and $\varepsilon = r_y/r_x$ is the ellipse aspect ratio.

On the β-plane, the exterior streamfunction field – a solution to (3) – dies out exponentially at infinity and, at the separatrix Γ, obeys the condition

$$\psi^{(Ex)}\big|_\Gamma = -Ur\sin\theta|_\Gamma, \tag{7}$$

where r and θ are polar coordinates ($x = r\cos\theta$, $y = r\sin\theta$). We seek it as a Fourier–Bessel series:

$$\psi^{(Ex)} = \psi^{(Ex)}(r, \theta) = \sum_{n=0}^{\infty} A_{2n+1} K_{2n+1}(lr)\sin(2n+1)\theta, \tag{8}$$

where K_ν is the ν-order modified Bessel function. When Γ is a circle of radius a, (7) and (8) provide the familiar Larichev–Reznik solution to the exterior problem:

$$\psi^{(Ex)} = -\frac{Ua}{K_1(la)} K_1(lr)\sin\theta.$$

For non-circular separatrices, the convergence is guaranteed outside the minimal circle enclosing Γ, but whether or not the series (8) converges in between this circle and the separatrix depends on the form of the latter. In the case of elliptical separatrices, some insight into the problem of convergence gives an inspection of the f-plane solution (6).

Consider an exterior f-plane solution given by (6*a*) or (6*b*) and extend it to the whole (x, y)-plane. Further, take its formal harmonic series

$$\psi^{(Ex)} = \sum_{n=0}^{\infty} A_{2n+1} \frac{1}{r^{2n+1}} \sin(2n+1)\theta. \tag{9}$$

Equations (6) are singular along the intervals connecting the foci of the corresponding ellipses. Therefore, series (9) converges only outside the circle passing through the ellipse foci (cf. Brazier-Smith 1984), and the necessary and sufficient condition for the convergence of series (9) everywhere outside Γ is that this circle is enclosed in Γ. In terms of the separatrix aspect ratio, this condition is: $1/\sqrt{2} < \varepsilon < \sqrt{2}$. Clearly, some limitation of this kind must exist for the β-plane elliptical modons as well, guaranteeing the convergence of series (8) for mildly extended ellipses.

In practical computations on the β-plane, we truncate series (8), replacing the infinite sum with a sum from $n = 0$ to N, and find the $N + 1$ unknown coefficients A_1 to A_{2n+1} by satisfying the boundary condition (7) in a fixed finite set of boundary points and solving the corresponding linear system of equations in the least-squares (LSQ) sense (for details see Kizner *et al.* 2003). To estimate the range of aspect ratios safe in the sense of convergence of series (8), we ran high-precision (31 decimal places) tests with N varying from 7 to 19 at $\beta r_x r_y/U \leqslant 1$ (independent non-dimensional parameters governing the elliptical modon solutions are discussed in § 2.4). Our tests showed that, at least within the interval $0.75 \leqslant \varepsilon \leqslant 1.25$, the computed maximum absolute value of $\Psi^{(Ex)}|_\Gamma$ over $0 \leqslant \theta \leqslant \pi/2$ is extremely small and decreases with growing N (table 1); it also decreases with decreasing U and ε approaching 1. These facts evidence in favour of the convergence of series (8) everywhere at the elliptical separatrix Γ and outside it for reasonable translation speeds and for ε varying within the interval $0.75 \leqslant \varepsilon \leqslant 1.25$. The results presented below correspond to this range of the aspect ratios.

N	$\varepsilon = 0.75$	$\varepsilon = 1.25$
7	2.390×10^{-4}	4.745×10^{-5}
9	5.000×10^{-5}	6.363×10^{-6}
11	1.097×10^{-5}	8.946×10^{-7}
13	2.489×10^{-6}	1.301×10^{-7}
15	5.791×10^{-7}	1.941×10^{-8}
17	1.376×10^{-7}	2.954×10^{-9}
19	3.315×10^{-8}	4.569×10^{-10}

TABLE 1. Maximal values of $|\Psi|$ at the modon separatrix.

2.3. *Interior solution*

Once the exterior solution is known, the second of the boundary conditions (5) becomes definite, and the problem (4), (5) is fully set. Based on the analogy with the circular modons, we can expect that conditions (5) determine a countable set of solutions to (4) in the domain bounded by Γ. Indeed, it is common knowledge that (4) implies a functional dependence between $q^{(In)}$ and $\Psi^{(In)}$. In circular modons, only linear relations $q^{(In)} = -k^2\Psi^{(In)}$ can hold (Kizner *et al.* 2003). In this case, there is a countable spectrum of values ka allowing the required matching of the interior and exterior solutions at the circular separatrix $r = a$ (Lamb 1932; Larichev & Reznik 1976). More specifically, on the f-plane, the allowed values of ka are roots of the first-order Bessel function J_1. On the β-plane, any fixed value of la determines a countable number of ka values. The latter means that the modon size a and its translation speed U are interrelated in circular β-plane modons. For this reason, the equations determining the parameter k in circular modons (both on the β- and f-plane) are conventionally referred to as dispersion relations. When the lowest branch of the dispersion relation is considered, i.e. when the smallest value of ka is taken, the corresponding circular modon is a pure dipole. Otherwise, the solution constructed on a higher branch of the dispersion relation, represents a dipole encircled in one or more circular rings of alternating vorticity; each ring is antisymmetric about the x-axis, i.e. consists of two semi-rings in which the vorticity is opposite in sign. Solutions of this type are sometimes referred to as 'shielded' modons. They, however, should not be confused with the shielded dipoles that are considered in § 3.1.

A detailed description of the general method for constructing baroclinic nonlinear interior solutions (including thorough accuracy estimates) appears in Kizner *et al.* (2003). Here, a brief overview of the method is given with special reference to barotropic elliptical modons.

We search for the interior solution using a version of the successive linearization (Newton–Kantorovich) iterative procedure and a collocation method with a polynomial approximation of the 'co-moving streamfunction'. Let i be the iteration index ($i = 0, 1, \ldots$). Once the ith approximation, $\Psi_i^{(In)}$, is known, approximation $i+1$ is computed as $\Psi_{i+1}^{(In)} = \Psi_i^{(In)} + \delta$, where the correction δ satisfies the third-order linear differential equation

$$J\left(\delta, q_i^{(In)}\right) + J\left(\Psi_i^{(In)}, \Delta\delta\right) = -J\left(\Psi_i^{(In)}, q_i^{(In)}\right) \tag{10}$$

and the boundary conditions

$$\delta|_\Gamma = -\Psi_i^{(In)}\big|_\Gamma, \quad \left.\frac{\partial}{\partial n}\delta\right|_\Gamma = \left.\frac{\partial}{\partial n}\Psi^{(Ex)}\right|_\Gamma - \left.\frac{\partial}{\partial n}\Psi_i^{(In)}\right|_\Gamma. \tag{11}$$

N	Mean res, eq. (10)	Mean Ψ_Γ	Mean $\left[\dfrac{\partial\Psi}{\partial n}\right]_\Gamma$	Mean q_Γ
7	0.037874	0.138762	0.037882	4.443335
9	0.026870	0.053644	0.034347	0.412563
11	0.009145	0.008515	0.003870	0.022257
13	0.001272	0.004962	0.001056	0.011988
15	0.000755	0.004373	0.000940	0.010306

TABLE 2. Root-mean-square errors in an ordinary β-plane modon solution ($\varepsilon = 1.15$).

Formally, starting from the second iteration, the right-hand parts in these conditions should be zero; however, because the linear problem is solved numerically, we use the above form at every iteration just to raise the accuracy. The above iterative procedure converges to a true solution of the problem (4), (5) if the initial guess $\Psi_0^{(In)}$ is chosen sufficiently close to this solution (Kantorovich 1948). While searching for a weakly elliptical dipole, we use as an initial guess the analytical Lamb–Chaplygin or Larichev–Reznik dipole solution with a circular separatrix of a radius $\bar{r} = \sqrt{r_y r_x}$ and translation speed U. In a similar manner, weakly elliptical solutions already found are used as initial guesses for computing dipolar modons with stronger elliptisities.

To facilitate the subsequent computations, we approximate the field $\Psi_0^{(In)}$ by a $(2N+1)$-degree polynomial in x, y, which is even in x and odd in y. The correction δ is represented in the same form:

$$\delta_{BT} = \sum_{0 \leqslant p+s \leqslant N} \alpha_{p,s} x^{2p} y^{2s+1}. \tag{12}$$

Now that the functions $\Psi_0^{(In)}$ and δ are given in polynomials, all differential operators appearing in (10) and (11) can be expressed explicitly. We require (10) and boundary conditions (11) to be satisfied in a chosen set of internal and boundary points, the number of points exceeding considerably the number of polynomial coefficients in (12). In this way, (11) and (12) are reduced to an over-determined system of linear equations in $\alpha_{p,s}$, which is solved in the LSQ sense. The LSQ approach assures that the linear system is well-determined; it provides a good approximation to the true exact solution everywhere within Γ by damping down the possible 'high-frequency' oscillations of the polynomials.

Because, in the barotropic case, fewer conditions (as compared to the baroclinic model) must be fulfilled, we were able to compute and study a sufficiently wide family of solutions. In most of these computations we used $N = 11$, approximately 700 internal points (i.e. a 30×30 mesh) and 300 boundary points; as seen from tables 1 and 2, this choice provides a sufficient accuracy. For checking the accuracy at which (4) was satisfied, a fine 200×200 mesh coating the first quadrant ($0 \leqslant x \leqslant r_x, 0 \leqslant y \leqslant r_y$) was used, while the fulfilment of boundary conditions along the first quarter of the separatrix was checked in 1000 points. In table 2, results of such a check are presented, the modon parameters being $\varepsilon = 1.15, \bar{r} = 1, U = 1$. In the headings of table 2, the following notations are used: 'Mean res, eq. (10)' is the root-mean-square residual, i.e. the mean (over about 31 400 fine-mesh points) of the right-hand part of (10) at the output of the iterative procedure; 'Mean Ψ_Γ' – the root-mean-square (over 1000 boundary points) of Ψ at the separatrix; 'Mean q_Γ' – the same for q; 'Mean $[\partial\Psi/\partial n]_\Gamma$' – the same for the jump of the normal to Γ

derivative of Ψ. In the special case of high translation speeds, computations were run with $N = 13$ (see § 3.1.1). We note that, the closer ε is to 1, the higher is the accuracy at which the interior solution is computed: for a circular modon, the errors are of the order of 10^{-10} at $N = 7$ and decrease with increasing N.

2.4. *Independent non-dimensional parameters*

As mentioned in § 1, only dipolar modons are considered in this paper. To understand how many free parameters define a translating elliptical modon (or, more generally, a modon with a convex symmetrical separatrix), it is convenient to rewrite the equation of vorticity conservation in a non-dimensional form using, for example, the geometrical mean radius of the vortex, $\bar{r} = \sqrt{r_y r_x}$, as a scale for x, y, r, and $\bar{r}U$ for ψ. In this case, on the β-plane, we have

$$J(\psi + y, \Delta\psi + \lambda^2 y) = 0, \quad \lambda^2 = \frac{\beta \bar{r}^2}{U}. \tag{13}$$

In non-dimensional variables, for the exterior domain we have: $q^{(Ex)} = \lambda^2 \Psi^{(Ex)}$ and $\Delta\psi^{(Ex)} = \lambda^2 \psi^{(Ex)}$, where $\lambda = l\bar{r}$; this form of the $q^{(Ex)}$ *vs.* $\Psi^{(Ex)}$ relation is independent of the separatrix shape. In the interior, the functional relation F_Γ between $q^{(In)}$ and $\Psi^{(In)}$, i.e. $\Delta\psi^{(In)} + \lambda^2 y = F_\Gamma(\psi^{(In)} + y)$, does depend on Γ (for example, for a circular modon, the function F_Γ is linear, and otherwise is nonlinear); here and below, the subscript Γ indicates the 'parametric' dependence of this relation on the separatrix form.

For translating modons on the f-plane, (1) in the non-dimensional variables becomes: $J(\psi + y, \Delta\psi) = 0$, yielding (2) outside the vortex frontier and a nonlinear dependence $\Delta\psi^{(In)} = F_\Gamma(\psi^{(In)} + y)$ in its interior.

In the case of a standing modon on the β-plane, the scale $\bar{r}U$ for ψ introduced above is invalid since $U = 0$. Instead, this time ψ should be scaled via $\beta\bar{r}^3$. The resulting non-dimensional form of (1) is $J(\psi, \Delta\psi + y) = 0$, so that $\psi^{(Ex)} = \Delta\psi^{(Ex)} = 0$ in the exterior and $\Delta\psi^{(In)} + y = F_\Gamma(\psi^{(In)})$ in the interior. Clearly, these scales are also appropriate for translating modons on the β-plane. If they are assumed, the non-dimensional version of (1) is

$$J\left(\psi + \frac{1}{\lambda^2} y, \Delta\psi + y\right) = 0, \tag{14}$$

which is equivalent to (13).

The above scaling indicates that, on the β-plane, two independent factors determine a translating modon solution, namely, λ^2 (incorporating the modon size and speed) and the vortex frontier shape (not size), whereas for standing modons on the β-plane and for translating modons on the f-plane, the separatrix shape is the only governing factor. In elliptical vortices, the aspect ratio ε can be chosen as the parameter determining the frontier shape.

All the results presented below are given in non-dimensional variables.

3. Stationary modon solutions

3.1. *β-plane elliptical modons*

3.1.1. *Classification of translating modons*

On the β-plane, the family of translating elliptical modons is two-parameter, the parameters being ε and λ^2. We constructed stationary modon solutions for $0 < \lambda^2 \leqslant 5$

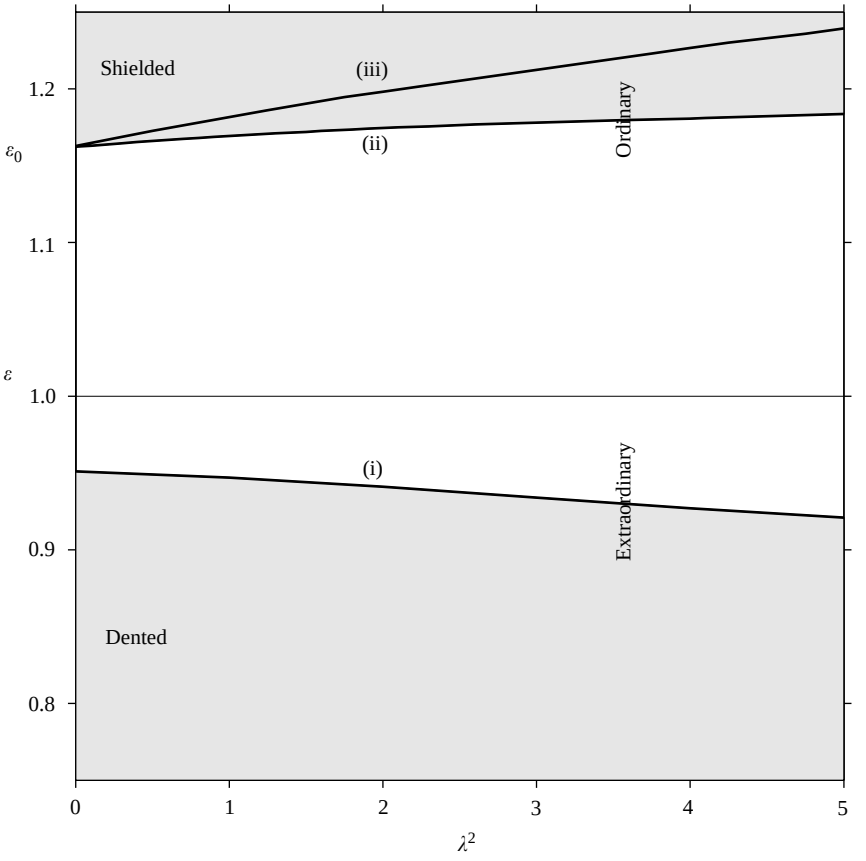

FIGURE 1. Classification of elliptical β-plane modons on the parameter plane (λ^2, ε): line (i) demarcates the regions of dented and non-dented solutions; line (ii), intermediate solutions between shielded and non-shielded modons; line (iii), supersmooth modons; shaded regions, dented (beneath line (i)) and shielded (above line (ii)) solutions; $\varepsilon_0 \approx 1.162$, aspect ratio of the f-plane 'supersmooth' elliptical solution.

and $0.75 \leqslant \varepsilon \leqslant 1.25$, the goals being to classify the possible dipole solutions according to the peculiarities of their vorticity fields and study the degree of nonlinearity of the function $q^{(In)} = F_\Gamma(\psi^{(In)})$ in relation to ε and λ^2. The main results of our analysis are summarized in figure 1, where the classification of modons in the parameter space (ε, λ^2) is shown. A detailed description of the solutions found is given below (see also figures 2 to 7).

As mentioned above, the circularity of the separatrix ($\varepsilon = 1$) and the linearity of the function F_Γ are equivalent properties of a β-plane modon. Boyd & Ma (1990), who considered the f-plane case and studied elliptical modons extended in the x-direction, noticed that the increase of ellipticity results in growing nonlinearity of the internal q *vs.* Ψ dependence. We found this to be true also on the β-plane both for ellipses extended in the x-direction and for those extended in the y-direction. Following the terminology of Kizner *et al.* (2003), we refer to the ellipses extended in the y-direction as 'ordinary' since these are the dipoles that usually emerge in laboratory and numerical experiments (see also § 4); correspondingly, the ellipses extended in the x-direction are termed 'extraordinary' (figure 1).

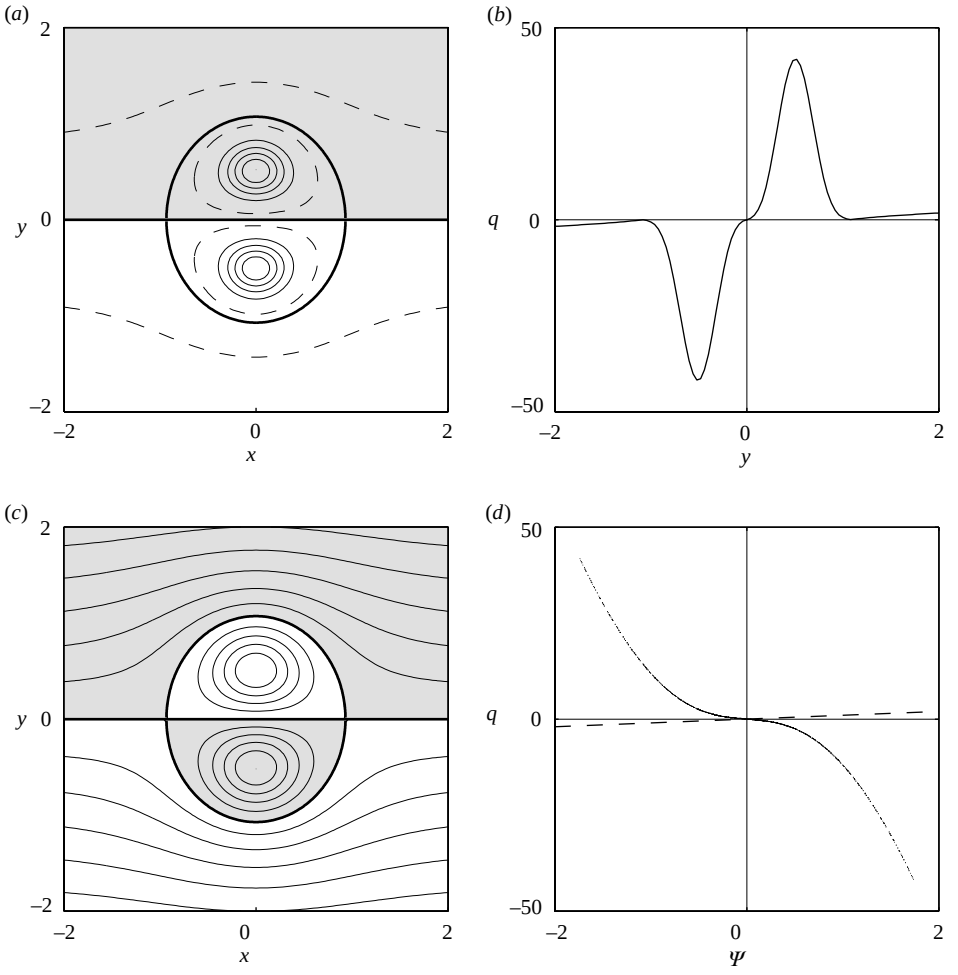

FIGURE 2. Ordinary β-plane elliptical modon (aspect ratio $\varepsilon = 1.15$; mean radius $\bar{r} = 1$; translation speed $U = 1$): (*a*) absolute vorticity q; (*b*) cross-section of the q field at $x = 0$; (*c*) 'co-moving streamfunction' Ψ; (*d*) q *vs.* Ψ scattergraph. Solid iso-contours in (*a*) and (*c*) are given at a 20% interval of the maximum/minimum; dashed contours, 2% of the maximum/minimum; bold line, zero contour; regions of positive values are shaded. Curved line in figure (*d*) corresponds to the interior domain; dashed straight line, exterior domain.

In ordinary elliptical modons, both $\Psi^{(In)}$ and $q^{(In)}$ assume their global maximum or minimum values at the modon poles (figure 2). Hereinafter the term 'pole' is used to designate the isolated extreme points of the fields $\Psi^{(In)}$ and $q^{(In)}$, i.e. those points in whose vicinity the iso-contours of $\Psi^{(In)}$ and $q^{(In)}$ are closed; these points should not be confused with the ellipse foci. In extraordinary modons, from a certain aspect ratio $\varepsilon = \varepsilon_D(\lambda^2) < 1$ down, the absolute vorticity field is 'dented' in the vicinity of the modon poles (figure 3); in these points $q^{(In)}$ assumes its local extrema, while the global maximum and minimum of $q^{(In)}$ are assumed at some closed contours encircling the poles; the $\Psi^{(In)}$ field remains qualitatively similar to that of a conventional circular modon. In figure 1, the line $\varepsilon = \varepsilon_D(\lambda^2)$ separating the regions of dented and non-dented extraordinary elliptical modons is labelled (i).

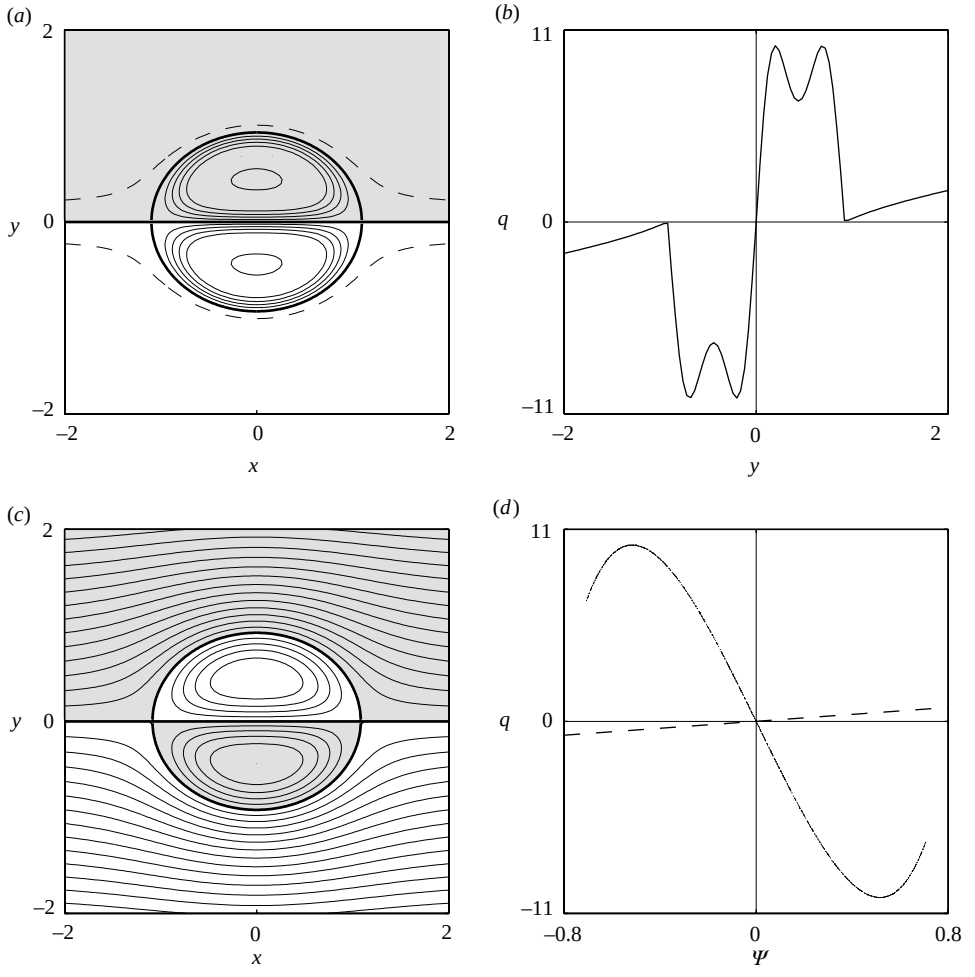

FIGURE 3. Dented extraordinary β-plane elliptical modon (aspect ratio $\varepsilon = 0.85$; other parameters and notation as in figure 2).

In ordinary elliptical modons, by increasing ε at fixed λ^2, increasingly curved $q^{(In)}$ *vs.* $\Psi^{(In)}$ scattergraphs were obtained (figure 4). There is a specific aspect ratio $\varepsilon = \varepsilon_{Sh}(\lambda^2)$ at which the scattergraph is tangent to the Ψ-axis while at $\varepsilon > \varepsilon_{Sh}(\lambda^2)$ the scattergraph crosses the Ψ-axes three times, and the modons become 'shielded' in terms of q; these 'shielded' modons remain two-polar, but each of the absolute vorticity patches of common sign (those including the poles) is enclosed in a region where q is oppositely signed (figure 5). We note that the physical and topological nature of shields in elliptical dipolar modons differs completely from that in the four-polar shielded circular Larichev–Reznik modons constructed on the second branch of the dispersion relation (see § 2.3) or in the four-polar elliptical solutions obtained in the vicinity of such circular modons (similar baroclinic solutions were described in Kizner *et al.* 2003). The line demarcating shielded and non-shielded modons on the (ε, λ^2)-plane is labelled (ii) in figure 1.

The functional dependence of q upon Ψ in the interior domain can be approximated at any accuracy by polynomials. Since $F_\Gamma(\Psi^{(In)})$ is an odd function, for every

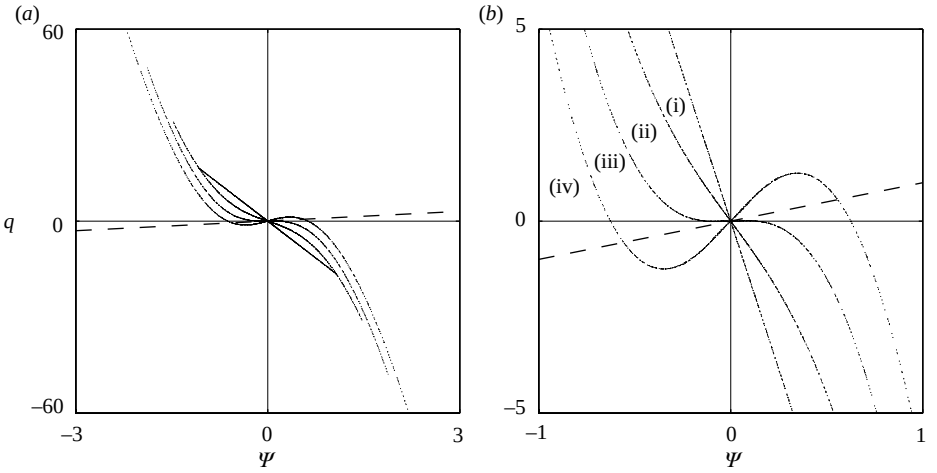

FIGURE 4. Scattergraphs (q *vs.* Ψ) of the circular and ordinary elliptical β-plane modons characterized by different aspect ratios (mean radius $\bar{r} = 1$, translation speed $U = 1$): (*a*) general view; (*b*) graphs in the vicinity of the origin; line (i), $\varepsilon = 1$; line (ii), $\varepsilon = 1.1$; line (iii), $\varepsilon = 1.175$; line (iv), $\varepsilon = 1.25$ (other notation as in figure 2*d*).

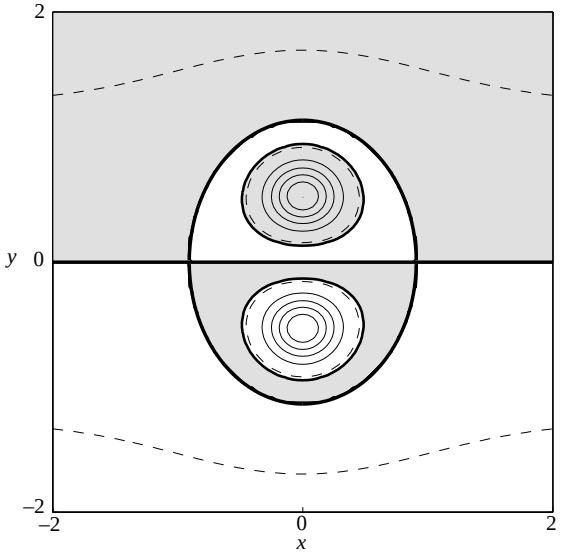

FIGURE 5. Shielded modon, q field (β-plane, aspect ratio $\varepsilon = 1.25$, mean radius $\bar{r} = 1$, translation speed $U = 1$; notation as in figure 2*a*).

solution found we approximated the interior scattergraph by an odd seventh-degree polynomial,

$$q = a_1\Psi + a_3\Psi^3 + a_5\Psi^5 + a_7\Psi^7, \tag{15}$$

and examined the dependences of the polynomial coefficients on λ^2 and ε. The most informative are the coefficients a_1 and a_3. Coefficient a_1 represents the slope at which the graph of the function $q = F_\Gamma(\Psi^{(In)})$ passes through the origin (figure 4). Regarding the coefficient a_3, computations show that in elliptical modons (when $\varepsilon \neq 1$) it differs from zero and carries the main information on the nonlinearity of the function

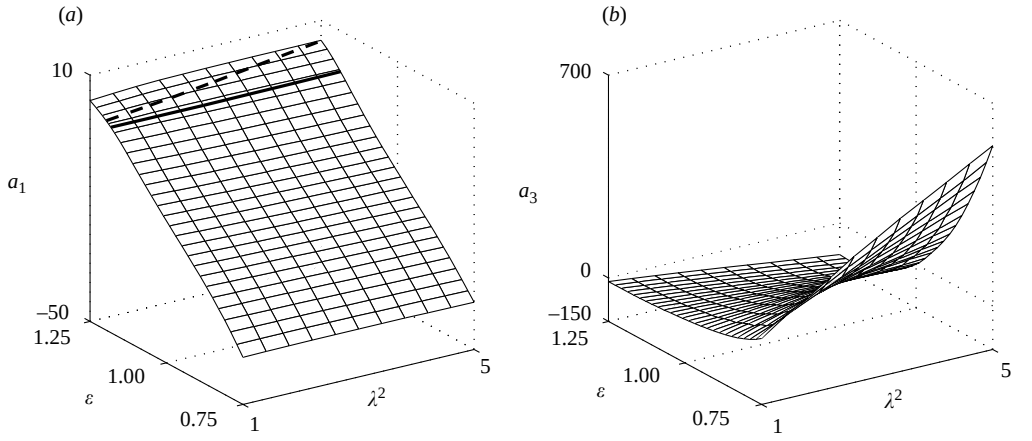

FIGURE 6. Characteristics of the internal q *vs.* Ψ scattergraphs of β-plane elliptical modons as functions of ε and λ^2: (*a*) slope in the origin (coefficient a_1 in (15)); bold solid line, $a_1 = 0$; bold dashed line, $a_1 = \lambda^2$; (*b*) nonlinearity index (coefficient a_3 in (15)).

$F_\Gamma(\Psi^{(In)})$, this is the reason to hold it as a nonlinearity index. We have restricted ourselves to the seventh degree in (15) because further increase in the degree did not affect significantly the coefficients a_1 and a_3.

As expected, in circular modons, the obtained internal q *vs.* Ψ scattergraphs are linear (i.e. $a_3 = a_5 = a_7 = 0$ at quite a high accuracy). Accordingly, the computed dependence of a_1 on λ^2 faithfully reproduces the first branch of the Larichev–Reznik dispersion relation considered in terms of $-(ak)^2$ and $(al)^2$. The surfaces visualizing the dependences of a_1 and a_3 on λ^2 and ε are shown in figure 6; they are based on computations at $N = 11$. As seen in figure 6(*b*), the nonlinearity increases with the deviation of ε from 1 (at fixed λ^2) and also with the increasing λ^2 (at a fixed ε) when, say, the translation speed decreases at fixed size and aspect ratio.

In figure 6(*a*), the bold lines superimposed on the surface $a_1 = a_1(\varepsilon, \lambda^2)$ represent the solutions that satisfy the conditions $a_1 = 0$ (solid line) and $a_1 = \lambda^2$ (dashed line). All the solutions that satisfy the condition $a_1 = 0$ fulfil the relation $\varepsilon = \varepsilon_{Sh}(\lambda^2)$; these are the solutions that demarcate shielded and non-shielded elliptical modons. The solutions that fulfil the condition $a_1 = \lambda^2$ constitute the class of so-called supersmooth elliptical solutions which are examined more closely in § 3.2.

The surfaces $a_1(\varepsilon, \lambda^2)$ and $a_3(\varepsilon, \lambda^2)$, shown in figure 6, stop at $\lambda^2 = 1$. This is due to the growing errors in the numerical procedure at decreasing λ^2. The accuracy could, in principle, be improved by raising N from 11 to 13 and by increasing the number of internal and boundary points in which the fulfilment of (10) and (11) are demanded. Because of the large volume of computations, we performed such high-accuracy calculations only for $\lambda^2 < 1$ and $1.14 < \varepsilon < 1.18$ and for $\lambda^2 < 1$ and $0.94 < \varepsilon < 0.96$. This was done in order to resolve the apparent meeting point of the two bold lines on the surfaces $a_1(\varepsilon, \lambda^2)$, and the point, in which line (i) in figure 1 runs into the axis λ^2. We note that, whenever the procedure converges at $N = 11$ and relatively coarse grid, the solutions obtained practically coincide with those obtained at higher N and finer grids.

3.1.2. *Supersmooth β-plane modons*

Consider now the slope at which the graph of the function $q^{(In)} = F_\Gamma(\Psi^{(In)})$ crosses the Ψ-axis in the origin. As seen in figures 4(*b*) and 6(*a*), this slope is a monotonic

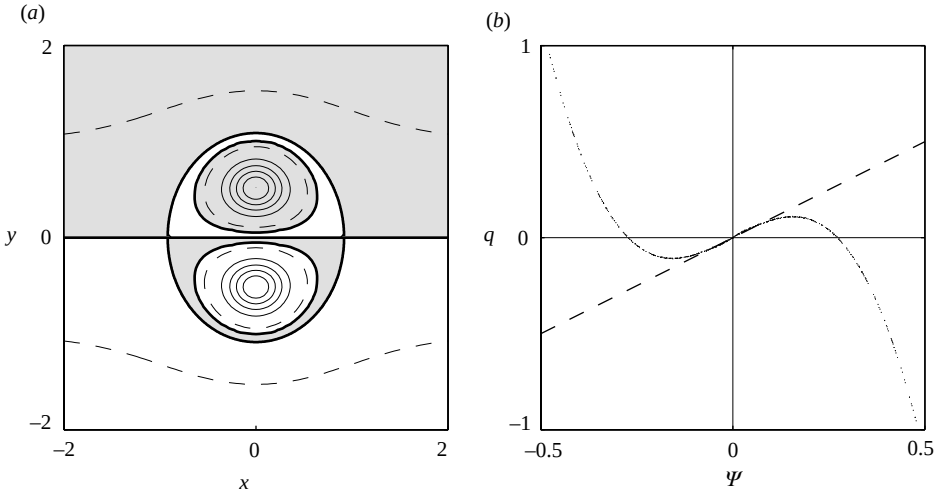

FIGURE 7. Supersmooth β-plane elliptical modon (aspect ratio $\varepsilon = 1.185$, mean radius $\bar{r} = 1$, translation speed $U = 1$): (*a*) iso-contours of q; (*b*) q *vs.* Ψ scattergraph in the vicinity of the origin (notation as in figure 2*a*, *d*).

function of ε; it is negative at $\varepsilon < \varepsilon_{Sh}(\lambda^2)$ and exceeds λ^2 when ε is large enough. Therefore, at any fixed λ^2, there exists a unique ordinary elliptical solution, in which the slope of the internal scattergraph in the origin equals that of the external graph,

$$\left.\frac{\mathrm{d}q^{(In)}}{\mathrm{d}\Psi^{(In)}}\right|_{\Psi^{(In)}=0} = \frac{\mathrm{d}q^{(Ex)}}{\mathrm{d}\Psi^{(Ex)}} \equiv \lambda^2. \tag{16}$$

This is the only elliptical modon with continuous normal vorticity derivatives at the separatrix, because (16) guarantees that

$$\left.\frac{\partial}{\partial n} q^{(In)}\right|_{\Gamma} = \left.\frac{\partial}{\partial n} q^{(Ex)}\right|_{\Gamma}.$$

We term the solutions with such a degree of smoothness of their vorticity fields '*supersmooth modons*'. Clearly, in supersmooth modons a certain single-valued relation $\varepsilon = \varepsilon_{SS}(\lambda^2)$ between the parameters ε and λ^2 is fulfilled.

In terms of the coefficient a_1, supersmooth solutions satisfy the condition $a_1 = \lambda^2$ (dashed line in figure 6*a*). The line $\varepsilon = \varepsilon_{SS}(\lambda^2)$ representing supersmooth modons in the parameter space is labelled (iii) in figure 1; it is a projection on the plane (λ^2, ε) of the dashed bold line $a_1 = \lambda^2$ shown in figure 6. It lies entirely inside the region of 'shielded' elliptical modons bounded by line (ii) in figure 1. Line (ii), in turn, is a projection on the (λ^2, ε)-plane of the solid bold line $a_1 = 0$ shown in figure 6(*a*). The estimated coordinates of the meeting point of lines (ii) and (iii) are $\lambda^2 = 0$ and $\varepsilon \approx 1.162$.

It is worthy of emphasizing again that, as distinct from the f-plane, the exterior scattergraph of a β-plane modon appears as a positively sloping straight line passing through the origin. Therefore, for the tangency of the exterior and interior scattergraphs in the origin, the latter must cross the Ψ-axis more than once. In other words, a supersmooth β-plane modon is necessarily shielded (figure 7).

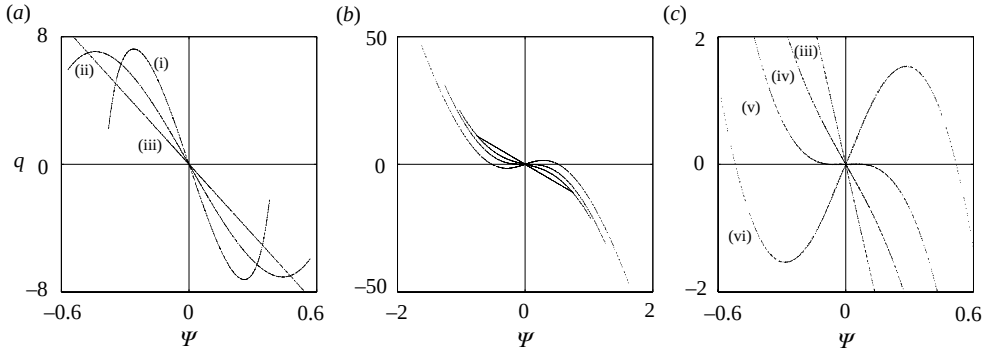

FIGURE 8. Scattergraphs (q *vs.* Ψ) in the interior domains of f-plane modons (mean radius $\bar{r}=1$, translation speed $U=1$): (*a*) extraordinary modons; (*b*) ordinary modons, general view; (*c*) ordinary modons, graphs in the vicinity of the origin; line (i), $\varepsilon=0.75$; line (ii), $\varepsilon=0.9$; line (iii), $\varepsilon=1$; line (iv), $\varepsilon=1.1$; line (v), $\varepsilon=\varepsilon_0\approx 1.162$; line (vi) $\varepsilon=1.25$.

3.1.3. *Standing β-plane modons*

The condition $U=0$ implies that, outside the separatrix, the streamfunction is zero, so the absolute vorticity is represented by the background, planetary vorticity y only (see § 2.2). On the other hand, owing to the antisymmetry, $q^{(In)}|_\Gamma = 0$. Therefore, standing elliptical β-plane modons, just like Stern's circular standing solution, possess a vorticity jump across the separatrix Γ. Ordinary and extraordinary standing solutions represent limiting cases of the corresponding translating modons as $\lambda^2 \to \infty$ (see (14)). We determined them by solving (4) numerically with zero boundary conditions and $\Psi^{(In)}$ replaced with $\psi^{(In)}$. In our computations, such modons were found only within the interval $0.85 \leqslant \varepsilon \leqslant 1.15$, their internal structures being qualitatively similar to those of the translating β-plane and f-plane modons at the same aspect ratio. The increase of the aspect ratio ε up to the maximal allowable value 1.15 did not lead to the formation of a vorticity shield (in the above-defined sense) around the poles. We might suppose that $\varepsilon \leqslant 1.15$ is simply insufficient for a β-plane modon to bear a shield. Does this result suggest that standing modons are always non-shielded (i.e. can only be mildly extended in the y-direction), or should it be interpreted as a limitation of the numerical procedure applied? To date, this question remains unanswered (even though the second alternative looks more likely).

3.2. *f-plane modons*

The elliptical f-plane modon solutions depend on a single free parameter, the aspect ratio ε. While in the exterior of such a modon $q=0$, the Ψ and q fields in the interior do not differ qualitatively from those of a modon on the β-plane. The nonlinearity of the function $F_\Gamma(\Psi^{(In)})$ increases with growing deviation of the aspect ratio from 1 (figure 8). This is also seen in figure 9 where the dependences of the coefficients a_1 and a_3 on ε in (15) for the f-plane elliptical modons are shown. When the aspect ratio is larger than a certain $\varepsilon_0 > 1$, the ordinary modons are shielded, otherwise they are non-shielded.

From the classification standpoint, the solution at $\varepsilon=\varepsilon_0$ (figure 9*a*) fulfils a twofold role: it both separates the shielded and non-shielded modons and is supersmooth. Indeed, in this solution $(\mathrm{d}q^{(In)}/\mathrm{d}\Psi^{(In)})|_{\Psi^{(In)}=0}=0$ and hence $(\partial/\partial n)q^{(In)}|_\Gamma = (\partial/\partial n)q^{(Ex)}|_\Gamma = 0$. This is distinctive from the β-plane case.

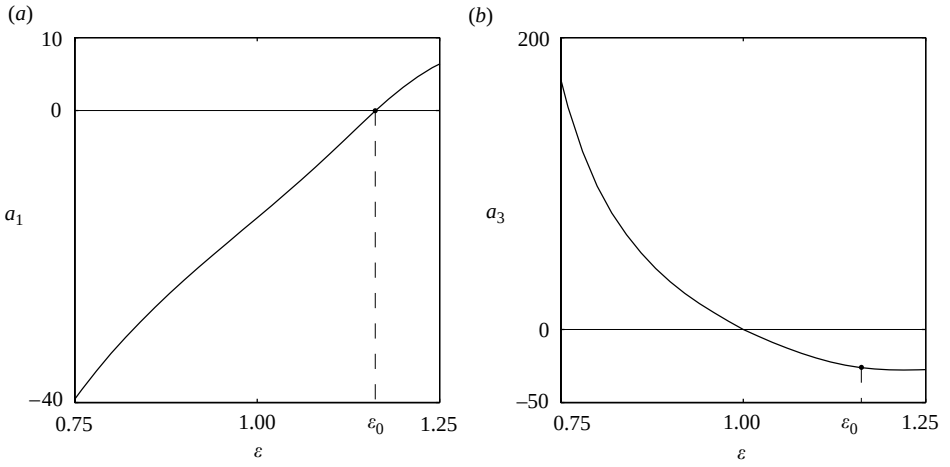

FIGURE 9. Characteristics of the internal q *vs.* Ψ scattergraphs of f-plane elliptical modons as functions of ε: (*a*) slope in the origin (coefficient a_1 in equation (15)); (*b*) nonlinearity index (coefficient a_3 in (15)); $\varepsilon = \varepsilon_0 \approx 1.162$, aspect ratio of the supersmooth modon.

On the β-plane, the two lines in the parameter space (λ^2, ε) symbolizing the supersmooth solutions and those separating the shielded solutions from non-shielded tend to meet at a point where $\lambda^2 = 0$ and $\varepsilon \approx 1.162$ (figure 1, lines (ii) and (iii)). Therefore, it comes as no surprise that an independent estimation of the aspect ratio $\varepsilon = \varepsilon_0$ separating the shielded and non-shielded modons on the f-plane gives the same value, $\varepsilon_0 \approx 1.162$: the β-plane supersmooth elliptical solutions and the intermediate solutions separating the shielded and non-shielded modons go to the above-mentioned supersmooth f-plane solution as $\beta \to 0$.

In a similar way, the f-plane solution that separates the dented and non-dented modons (at $\varepsilon \approx 0.951$) can be thought of as a limiting case (as $\beta \to 0$) of the β-plane modon solutions represented in figure 1 by line (i).

4. Temporal evolution of circular and elliptical modons

4.1. *Simulation model*

4.1.1. *Base version*

To clarify the stability properties of the solutions obtained, we conducted a series of numerical experiments in which temporal evolution of modons was followed, resulting from different kinds of perturbations (see below). For this purpose we adopted the code previously used by Kizner & Berson 2000 (see also Kizner *et al.* 2002, where a more general, multi-layer version of this model is described in detail). The model was initialized using the stationary elliptical modon solutions presented above, the variables being non-dimensional.

Since a β-plane elliptical modon is determined by only two independent parameters ε and λ^2, when dealing with the β-plane, we can use the initial mean radius of the dipole $\bar{r}_0$ as the scale for the space variables x, y, r, and chose the following scales for the remaining variables: $U^* = \beta \bar{r}_0^2$ for the velocity, $T = \bar{r}_0 / U^*$ for time; $U^* \bar{r}_0$ for the streamfunction and $1/T$ for the vorticity. Clearly, such a scaling incorporates both travelling and standing β-plane modons. The non-dimensional β-plane simulation

model is based on two equations:

$$\frac{\partial q}{\partial t} + J(\psi, q) = 0 \tag{17}$$

and

$$\Delta\psi = q - y, \tag{18}$$

where t is time and x and y are the space coordinates in an absolute frame of reference.

Regarding the f-plane, since elliptical dipole modon solutions depend on only one free parameter ε, we can run experiments with modons having the same initial radius and the same initial translation speed U. By substituting this fixed initial translation speed for U^* and keeping the definitions of the remaining scales, we arrive at the same non-dimensional equation (17), whereas (18) is replaced by

$$\Delta\psi = q. \tag{19}$$

Equation (17) is integrated in a rectangular box $[-X < x < X; -Y < y < Y]$ with periodical conditions at $x = \pm X$, the conditions at $y = \pm Y$ being $\psi = 0$; the 'physical' x-coordinate is calculated as $x + 2Xn$, where n is the number of crossings of the right-hand boundary of the box by the modon centre. In all the experiments $X = Y = 5$, the mesh size equals 0.05, the time step τ is controlled by the gradients of ψ and q and varies within the interval 10^{-3} to 5×10^{-3}. The computations at any time step t comprise the following elements. First, the streamfunction ψ is determined from the Poisson equation (18) (β-plane) or (19) (f-plane) supplied with the corresponding boundary conditions. At this stage, the vorticity q is assumed from the previous time step $t - \tau$ (if $t > 0$) or from the initial condition (if $t = 0$), and the problem is solved using a spectral decomposition in eigenfunctions in the x-direction and marching in the y-direction. Subsequently, the vorticity is computed from the finite-difference analogue of (17), where a combination of the direct and Matsuno schemes and Arakawa approximation for the Jacobian operator are used (Mezinger & Arakawa 1976); this scheme conserves the net energy in the box.

Note that the zero-step streamfunction field computed according to the above-described algorithm will always differ a little from that of the high-resolution (nearly exact) stationary modon solution whose vorticity serves as the initial condition. This is a manifestation of the so-called 'adjustment error' – a result of the adjustment of the 'exact' solution to the larger mesh size and finite dimensions of the domain considered. Accordingly, the aspect ratio, ε, and the distance between the poles, d, estimated from Ψ and displayed in the figures as corresponding to $t = 0$ might differ slightly from their exact values. The translation speed is computed at $t = 0, 1, \ldots$ from the observed displacement of the Ψ maximum. Therefore, the estimated initial translation speed also differs somewhat from the prescribed value. To distinguish the modon parameters at $t = 0$ estimated in this way from the ones prescribed in our procedure for the construction of stationary modon solutions, we refer to the latter as 'nominal' parameters.

4.1.2. *Cutting filter*

When weakly non-stationary processes are simulated, i.e. when a modon evolves slowly in time while translating along the x-axis, the model can be used as it is. The situation changes noticeably if the modon behaves in an essentially non-stationary manner. In this case, owing to periodicity in the x-axis, the vortex can be bombarded by its own vorticity filaments or debris and, on the β-plane, by Rossby waves

emitted by itself. Clearly, such an evolution may differ significantly from that on an unbounded (x, y)-plane. To treat this problem, we adopt a version of the so-called cutting procedure suggested by Hesthaven, Lynov & Nycander (1993), which is akin to the 'contour surgery' (Dritschel 1988) conventionally used in the contour dynamics to cutoff long and thin vorticity filaments. Within the cutting procedure, periodically in time, a mask is put on the computed relative vorticity field, $\Delta\psi$, the period being equal to 1. The mask blots out the peripheral vorticity by replacing $\Delta\psi$ with $M(r)\Delta\psi$, where the function $M(r)$ equals 1 at $r \leqslant 3$ and smoothly decreases in a Gaussian manner as $r > 3$ becoming, in effect, zero at $r > 4$.

The periodical cutting has a different effect on the dynamics of the f-plane and β-plane modons. In terms of vorticity, non-stationary dynamics are primarily apparent in the distortion of the q field in the wake of a modon due to filamentation. Thus, on the f-plane, the exterior flow outside this wake remains irrotational ($q = \Delta\psi = 0$), and the mask, while cutting off the train of filaments and debris at $r > 4$, does not affect the modon core structure or its translational movement.

On the β-plane, the far-field structure and the translation speed of slowly (adiabatically) evolving modons are interrelated. Indeed, as seen from (3) and (8), when r is sufficiently large, a steady-state relative vorticity field is proportional to $\psi^{(Ex)}$ and hence must decay as an exponent of $r\sqrt{\beta/U}$ (in dimensional variables). Therefore, when a quasi-steady or weakly non-stationary stage of evolution is modelled, the main dynamical effect of cutting is a mild reduction of the modon translation speed with respect to that on an unbounded (x, y)-plane (the 'hindering effect' described by Kizner *et al.* 2002). At a strongly non-stationary stage, however, the reduction of translation speed due to the cutting becomes insignificant as compared to the effect of 'bombarding' if the cutting filter were not applied.

We ran a number of experiments, in which the temporal evolution of the elliptical modons was simulated. Two versions of the model were employed. The version without the cutting was used when dealing with slowly evolving (non-dented and non-tilted modons). In this case, we studied the resistance of the modons to small disturbances induced by the finite size of the basin, periodical conditions at its western and eastern boundaries, finite-difference approximation and processor rounding off. The experiments were then re-run with the application of cutting in order to clarify the effect of modon slowing down on the separatrix form and other modon characteristics. For vortices exhibiting conspicuous filamentation and Rossby wave radiation (dented modons on the f- and β-plane and tilted β-plane modons), only the version with the cutting was applied.

4.2. *Evolution of β-plane modons*

4.2.1. *Slowly evolving modons. Simulations without cutting*

Non-dented modons (those with $\varepsilon_D(\lambda^2) < \varepsilon$, see figure 1) being subjected to small perturbations change quite slowly; the timescale of these changes is much smaller than the characteristic turnover time. Therefore, it is appropriate to simulate their evolution without the cutting filter.

According to our computations, mildly extended modons (those with the separatrix aspect ratio ranging approximately from 0.95 to 1.05) behave qualitatively in the same manner as does the circular modon. The latter is known for its robustness tested in several numerical experiments (McWilliams & Flierl 1979; McWilliams *et al.* 1981; Makino, Kamimura & Taniuti 1981; Larichev & Reznik 1983; Hesthaven *et al.* 1995). However, these experiments, owing to their relatively short duration (tens of time

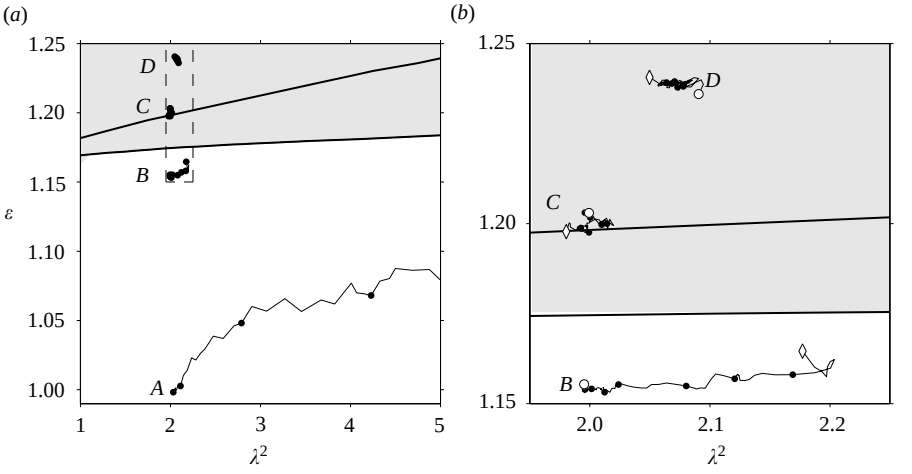

FIGURE 10. Evolution of the circular and ordinary elliptical β-plane modons in projection on the parameter plane (λ^2, ε), simulations without cutting: *A*, *B*, *C*, *D*, tracks left by evolving modons with the initial nominal aspect ratios 1, 1.15, 1.2 and 1.25, respectively, and $\lambda^2 = 2$; time separation between solid circles is 500. (*a*) General view; (*b*) magnified area of elliptical modons (enclosed in dashed rectangle in (*a*)); ○, initial states; ◇, states reached by $t = 4000$.

units), do not allow us to judge whether a circular modon is stable or is it an unstable slowly evolving coherent vortex structure.

Our experiments lasted for thousands of time units. The results related to the circular modons can be interpreted as a demonstration of their weakly unstable behaviour; the modon characteristics changed slowly, but rather monotonically. This can be seen, for example, in figure 10(*a*) (line A), where tracks left on the parameter plane (λ^2, ε) by four evolving modons are shown. It is worth noting that, in the experiments on the f-plane (see § 4.3), the circular Lamb modon also behaves somewhat unstably: it slows down regardless of whether the cutting is applied or not. This suggests that the slowing down observed in the translation of the initially circular β-plane modon with the nominal translation speed $U = 0.5$ is not just a result of 'bombarding', but is a manifestation of truly unstable processes in its dynamics that eventually lead to the disintegration of the dipole.

Ordinary elliptical modons whose evolution is shown in figure 10(*a*) have the same nominal translation speed $U = 0.5$ (i.e. $\lambda^2 = 2$), but different aspect ratios: $\varepsilon = 1.15$, $\varepsilon = 1.2$ and $\varepsilon = 1.25$. They demonstrate a more stable behaviour than the circular modon (figure 10*a*). Direct calculations show that, at a fixed translation speed, vortices with higher aspect ratios possess a larger amount of kinetic energy. However, this is not the reason for their generally stronger robustness as compared to the circular modons. Indeed, according to our data, an ordinary elliptical modon with nominal parameters $\varepsilon = 1.15$ and $U = 0.35$ that has the same integral kinetic energy (approximately 3.12) as the circular modon with $U = 0.5$, changes by $t = 1000$ less significantly than the circular modon.

A closer inspection of the tracks at a higher resolution (figure 10*b*) convinces us that the shielded modon with the initial nominal aspect ratio $\varepsilon = 1.2$ is the most stable (probably, the only stable) among the four dipoles tested. Throughout the whole simulation – for 4000 time units – this modon remains the closest (in the metrics of the (λ^2, ε)-plane) to its initial position and to the line $\varepsilon = \varepsilon_{SS}(\lambda^2)$ representing the supersmooth 'exact' modons, the distances being within the limits of the adjustment

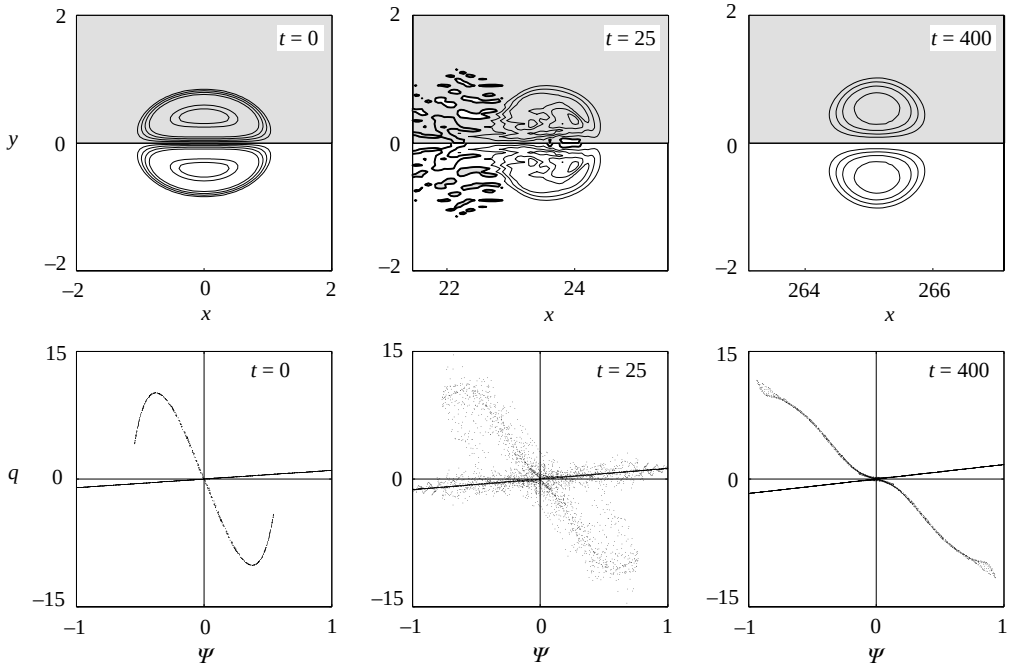

FIGURE 11. Evolution of an initially extraordinary dented elliptical β-plane modon (nominal mean radius $\bar{r} = 1$, translation speed $U = 1$, aspect ratio $\varepsilon = 0.75$): upper panel, q fields (notations as in figure 2*a*); lower panel, q *vs.* Ψ scattergraphs.

error (see § 4.1.1). We interpret this as evidence of the stability of supersmooth modons and attribute it to the continuity of the vorticity derivatives at the separatrices of such modons. In this relation, it is worth noting that, in non-supersmooth modons, the angle between the interior and exterior q *vs.* Ψ scattergraphs remains non-zero for thousands of time units.

In all the experiments presented in this subsection, the changes in net enstrophy do not exceed the limit of 0.5%.

4.2.2. *Simulations with cutting. Instability, slow evolution and shield formation*

According to our experiments, dented modons (those strongly extended in the x-direction) are unstable: the stronger the dent (i.e. the stronger the separatrix extension), the stronger the changes undergone by the dipole. Eventually, vortices of this kind make transitions to quasi-steady non-dented dipole states, in which the global maximum and minimum of q in the interior domain are assumed at the poles. In figure 11, such a transition is shown, the nominal aspect ratio and translation speed of the initial state being $\varepsilon = 0.75$ and $U = 1$, respectively. This vortex is essentially unstable: almost immediately a strongly non-stationary phase in its evolution begins, which is evidenced by filament emission and strong irregularities in the core vorticity field observed, e.g. at $t = 25$ (figure 11). To resolve the train of vorticity debris in the wake of the dipole, we have performed a separate short-term run ($t \leqslant 20$) without cutting, but in a longer basin ($X = 10$, $Y = 5$). It was found that the debris behind the dipole has a clearly periodical structure (the wavelength being approximately 2.5

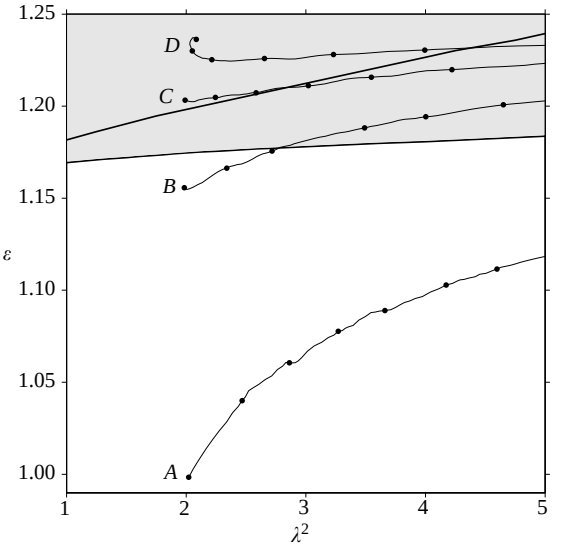

FIGURE 12. Evolution of the circular and ordinary elliptical β-plane modons in projection on the parameter plane (λ^2, ε), simulations with cutting; notations and initial parameters as in figure 10(*a*).

to 3) and slowly propagates westward; a similar periodicity was also viewed in the streamfunction field. From these observations, it can be deduced that a weak Rossby-wave radiation takes place (we, however, were unable to produce a reliable estimate of the phase speed). This conclusion is supported by the fact that no periodical structures were observed in the corresponding f-plane experiments (see § 4.3).

While undergoing these changes, the vortex slows down but, by $t = 100$, reorganizes into a well-formed quasi-stationary non-circular and non-dented dipole slightly extended in the y-direction ($\varepsilon \approx 1.03$), the peak values of q being approximately equal to the initial q maximum and minimum. The further nearly steady translation of the dipole (with a weak slowing down) was followed up to $t = 400$ (figure 11). The net enstrophy in this experiment decreases owing to the filament emission and the cutting applied, the loss of enstrophy by $t = 400$ being about 5% of the initial quantity. Regarding the form in which the modon stabilizes, it is clearly not an ellipse because the final scattergraph differs qualitatively from those of ordinary elliptical modons.

The above scenario is typical of dented extraordinary modons with sufficiently high initial translation speeds. Slower dented modons do not survive the strongly non-stationary phase and disintegrate. The closer the aspect ratio of an extraordinary vortex to $\varepsilon = \varepsilon_D(\lambda^2)$, the weaker its dent; correspondingly, the changes undergone by the vortex are less dramatic.

As noted in § 4.1.2, while with dented modons the use of the cutting procedure is unavoidable (for relatively small basins and long times), it is unnecessary when dealing with non-dented dipoles. Nevertheless, we found it instructive to run a series of experiments, in which the evolution of the ordinary modons considered in § 4.2.1 ($\varepsilon = 1$, $\varepsilon = 1.15$, $\varepsilon = 1.2$ and $\varepsilon = 1.25$) was simulated with the application of the cutting filter – just to understand the role of the latter better. The temporal evolutions of the key parameters of these four dipoles up to approximately $t = 3000$ are shown in figure 12 (tracks on the (ε, λ^2)-plane) and, in more detail, but for a shorter time period

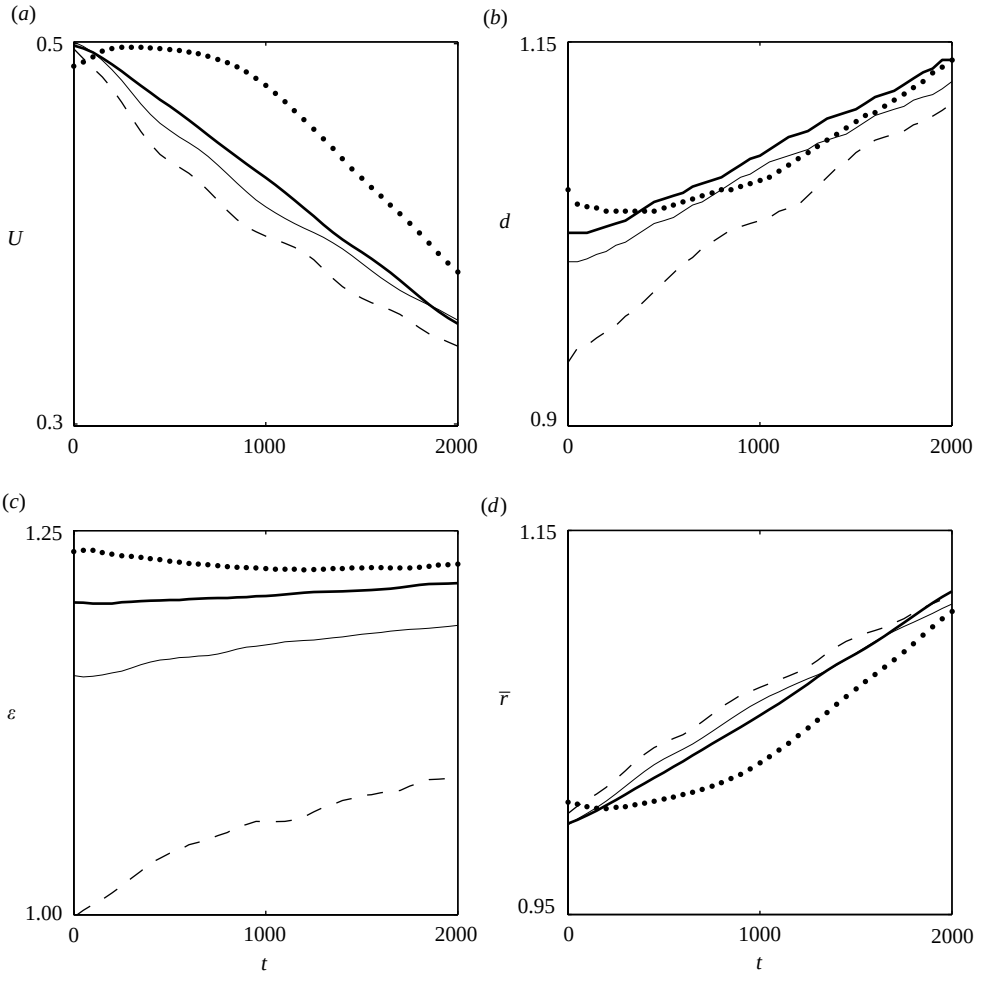

FIGURE 13. Evolution of parameters of the circular and ordinary elliptical β-plane modons (initial nominal radius $\bar{r}=1$; translation speed $U=0.5$ (i.e. $\lambda^2=2$)) in the simulations with cutting: dashed line, the modon with the initial nominal aspect ratio $\varepsilon=1$; thin solid line, $\varepsilon=1.15$; bold solid line, $\varepsilon=1.2$; dotted line, $\varepsilon=1.25$. The displayed parameters are: (*a*) translation speed U, (*b*) distance d between Ψ poles, (*c*) aspect ratio ε, (*d*) mean radius $\bar{r}$.

($t \leqslant 2000$) in figure 13. These data show that, up to $\varepsilon=1.2$, the form of modons with higher aspect ratios changes less significantly. Again, the circular modon undergoes the strongest changes, while the shielded modon with the nominal aspect ratio $\varepsilon=1.2$ turns out to be the least susceptible to the perturbations produced by the model.

As expected (§4.1.2), the cutting filter hinders the eastward propagation of the ordinary vortices; since the vortices change slowly, the loss of net enstrophy by $t=5000$ is within 2%. A new observation is that, in the experiments with the modons whose nominal aspect ratios were 1, 1.15 and 1.2, the decrease in translation speed is attended by a slow increase in the modon mean radius $\bar{r}$ (figure 13*a*, *d*), i.e. with the entrainment compensating the decrease in integral energy within the modon separatrix owing to the slowing down. The modon with the nominal aspect ratio 1.25, however, behaves in a different manner. Taking into account the hindering effect of

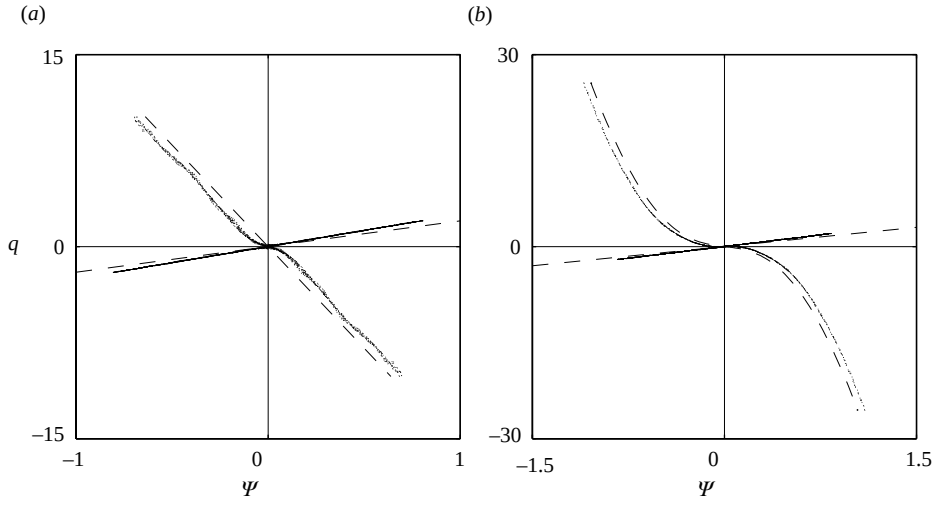

FIGURE 14. Scattergraphs (q *vs.* Ψ) of the quasi-steady states reached by two β-plane modons by $t = 1000$ in the experiments with cutting. The initial nominal parameters of the modons are: (*a*) $\lambda^2 = 2$ and $\varepsilon = 1$ (line A in figure 12 and dashed lines in figure 13); (*b*) $\lambda^2 = 2$ and $\varepsilon = 1.15$ (line B in figure 12 and thin solid lines in figure 13); dashed lines, q *vs.* Ψ relations at $t = 0$.

the cutting filter, the apparently small increase in the translation speed at the first stage of evolution of this modon ($t \leqslant 500$) should be regarded as a manifestation of essential acceleration of its eastward translation. This is physically consistent with the observed rapprochement of the modon's poles within the time interval $0 < t < 500$, diminishing of the separatrix aspect ratio and decrease of the mean radius (figure 13).

To summarize, the modons in these four experiments demonstrate a substantial resistance to the perturbing effect of the cutting filter, the evolution of the dipole with the initial nominal aspect ratio $\varepsilon = 1.2$ being the slowest. This slow evolution can be understood as an additional indication of the stability of the supersmooth solutions. In this regard, we note that, ideally, each Lagrangian particle must conserve its vorticity q and, hence, we can speak only of neutral stability. Accordingly, when considered in the parameter space, a stable modon subjected to such perturbations must not remain in the vicinity of the initial state, but can slowly recede from it, passing from one quasi-stable state to another. We believe this is what is actually observed in this experiment.

This brings us to another question: can the states passed by slowly evolving dipoles be described as ordinary elliptical modons? No certain answer can be given to this question. For instance, the dipole, whose q *vs.* Ψ relation is displayed in figure 14(*a*), is the state to which the circular modon evolved by $t = 1000$. Its internal scattergraph – two nearly straight lines linked by a short bar – differs qualitatively from that typical of elliptical modons. In another example (figure 14*b*), the scattergraph of the dipole that had been shaped by $t = 1000$ from an elliptical modon with the nominal aspect ratio $\varepsilon = 1.15$ and translation speed $U = 0.5$ has much in common with the q *vs.* Ψ graphs of ordinary elliptical modons. Moreover, following the evolution of each of the three elliptical modons shown in figure 12, we fitted explicit elliptical solutions to the observed values of U, $\bar{r}$ and ε at $t = 500, 1000, \ldots$ and found that, up to $t = 2000$, their scattergraphs were fairly similar to those of the evolving dipoles, including the peak

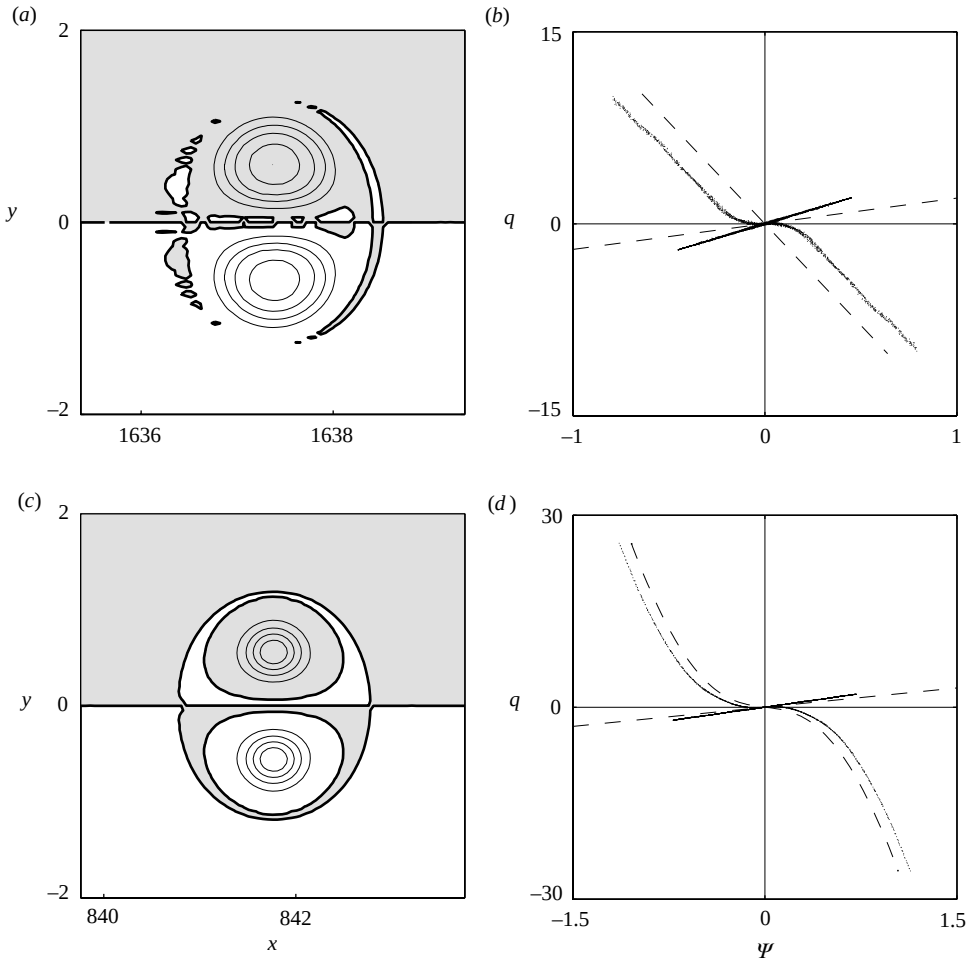

FIGURE 15. States achieved in the long-term evolution of two β-plane modons, simulations with cutting: (*a*), (*c*) q fields; (*b*), (*d*) q *vs.* Ψ scattergraphs; upper panel, initially circular modon (with nominal parameters as in figure 14*a*) at $t = 5000T$; lower panel, initially elliptical modon (with nominal parameters as in figure 14*b*) at $t = 2000T$; notation as in figure 11 (dashed lines in (*b*), (*d*), q *vs.* Ψ relations at $t = 0$).

values of Ψ and q. However, in the subsequent evolution, the discrepancy between the peak values of q gradually grew.

Our long-term simulations suggest that the periodical-in-time perturbations, induced by the cutting filter, gradually transform the circular dipole to such a state, which is more resistant to these perturbations in terms of the modon form (e.g. line *A* figure 12). It is possible that, in the long-term perspective, the dipole could achieve a 'supersmooth', though not exactly elliptical, steady state. In this process, the perturbations induced by the model can serve as a source of negative vorticity at $y > 0$ and positive vorticity at $y < 0$ required for the formation of shields (figure 15). The tendency towards a shield formation and approaching a 'supersmooth' state is especially evident in the evolution of the elliptical vortex with the nominal aspect ratio $\varepsilon = 1.15$ (figure 15*c*, *d*). In this case, the scattergraph of the dipole at $t = 2000$ (figure15*d*) is qualitatively similar to that shown in figure 7(*b*), but the dipole cannot

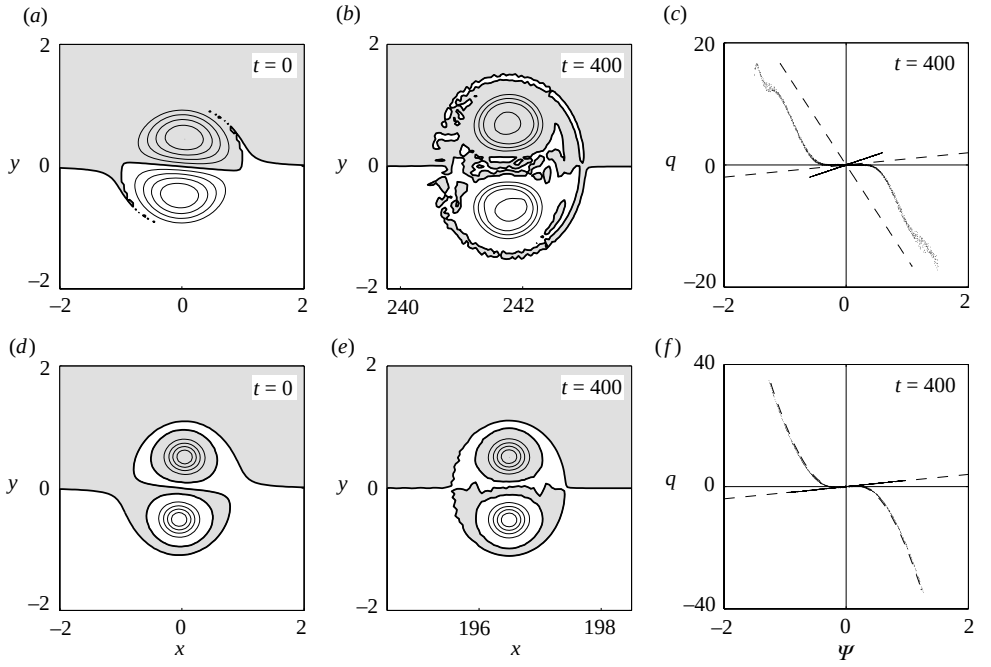

FIGURE 16. Experiments with modons tilted by 5° relative to the x-axis: upper panel, circular modon with the nominal translation speed $U = 1$; lower panel, elliptical modon with nominal parameters $\varepsilon = 1.2$ and $U = 0.5$; (*a*) and (*d*), absolute vorticity fields at the beginning of the experiments; (*b*), (*e*) same at $t = 400$ (notation as in figure 15*b*, *d*); (*c*), (*f*) q *vs.* Ψ scattergraphs (notation as in figure 2*d*, dashed lines, q *vs.* Ψ relations in the 'exact' solutions before tilting).

be categorized as an elliptical supersmooth modon as its estimated parameters ε and λ^2 do not fit the relation $\varepsilon = \varepsilon_{SS}(\lambda^2)$ (see figure 12).

So far, the perturbations considered were antisymmetric about the x-axis. For completeness sake, a few experiments with translating modons were run, in which small asymmetric perturbations were imposed on the initial states by tilting them by 5° relative to the x-axis. Since a tilted modon is not a stationary state, its evolution is evident from the very beginning. While translating generally eastward, the modon oscillates around the x-axis and emits vorticity filaments and Rossby waves. The latter makes necessary the application of the cutting filter.

Regarding the circular modons, our results were qualitatively similar to those of Hesthaven *et al.* (1993), who considered the behaviour of tilted divergent Larichev–Reznik modons at different initial translation speeds (see also Makino *et al.* 1981). A circular modon with the nominal translation speed $U = 0.5$ did not survive the perturbation and, despite the fact that by $t = 20$ its oscillations around the x-axis had actually died out, the dipole continued emitting vorticity filaments and Rossby waves, swiftly decelerated and eventually disintegrated by $t = 70$. In contrast, a circular modon with the nominal translation speed $U = 1$ did survive the initial perturbation (figure 16*a*–*c*). At the completion of the stage of detectable oscillation, by $t \approx 100$, the translation speed of the dipole was $U \approx 0.98$. Its subsequent evolution was similar to that of a non-tilted circular modon, however, the aspect ratio ε increased at a faster rate than in the non-tilted circular modon with nominal translation speed $U = 0.5$. As evidenced by figure 16(*c*), where the scattergraphs representing the interior and

exterior regions cross each other at a non-zero angle, by $t = 400$ there was still a certain vorticity jump at the vortex frontier. The enstrophy loss due to the cutting in this experiment was approximately 1.5%.

The ordinary elliptical dipoles with nominal parameters $U = 0.5$ and $\varepsilon = 1.15$, 1.2, 1.25 and the dipole with $U = 0.35$ and $\varepsilon = 1.15$ (whose energy is equal to that of the circular modon with $U = 0.5$) demonstrated a more stable behaviour in response to tilting, their post-oscillation evolution being similar to that of non-tilted modons with the same nominal parameters. Again, the change undergone by the modon with the nominal parameters $U = 0.5$ and $\varepsilon = 1.2$ was least of all. Accordingly, by $t = 400$, the enstrophy loss in this experiment was only about 0.1% of the initial amount. This modon has actually restored its initial characteristics within a few hundred time units (figure 16*d–f*). These results support the above conclusion regarding the stability of the supersmooth elliptical modons.

The evolution of a standing elliptical modon with the aspect ratio $\varepsilon = 1.1$ was also examined. The observed behaviour of this dipole was similar to the unstable evolution of the circular Stern modon described in detail by Kizner & Berson 2000 (see also § 1).

4.3. *f-plane modons*

The f-plane modons tested for stability differed in their initial aspect rations, the nominal translation speed being the same ($U = 1$). In outline, the results obtained on the β-plane remain valid on the f-plane: dented modons are unstable whereas non-dented modons evolve quite slowly.

The evolution of the dented modon with the initial parameters $\varepsilon = 0.75$ and $U = 1$ was modelled both with the cutting filter (up to $t = 400$) and without it (up to $t = 20$, but in a longer basin). The initial stage of the evolution was characterized by substantial filamentation. However, as distinct from the β-plane case, no clear-cut periodical structure was observed in the debris train behind the dipole.

A more detailed consideration is merited by the ordinary supersmooth modon (demarcating the shielded and non-shielded configurations) and a comparison of the evolution of vortices of these three types. The corresponding experiments were run both with and without the cutting and, in full agreement with our preliminary considerations (§ 4.1.2), no significant difference between the two versions was observed. The temporal variation of the key parameters of the modons with the nominal aspect ratios $\varepsilon = 1$ (circular); $\varepsilon = 1.16$ (supersmooth); and $\varepsilon = 1.25$ (shielded) is shown in figure 17 (simulations without cutting).

Within the period $0 < t < 1000$, the circular (Lamb) modon gradually extends in the y-direction, while slowing down and increasing the aspect ratio and mean radius (figure 17). Just as in the evolution of the Larichev–Reznik modon, the quasi-stationary states passed by the dipole were not exactly elliptical, since their internal q *vs.* Ψ dependences differed from those typical of elliptical modons. This vortex displays the greatest change in U, d and $\bar{r}$ among the three compared.

In contrast to the circular modon, the 'supersmooth' elliptical dipole ($\varepsilon = 1.162$) appears to be remarkably stable; all its characteristics – size, shape, translation speed, distance between the poles and q *vs.* Ψ relation) – remain nearly constant during the whole period $0 < t < 1000$. In this respect, it is analogous to the supersmooth β-plane modons.

Compared to the supersmooth modon, the shielded modon undergoes stronger changes. Three stages can be observed in its evolution. Within the first 300 time units, the modon evolves quite slowly. The changes in its parameters within the time interval

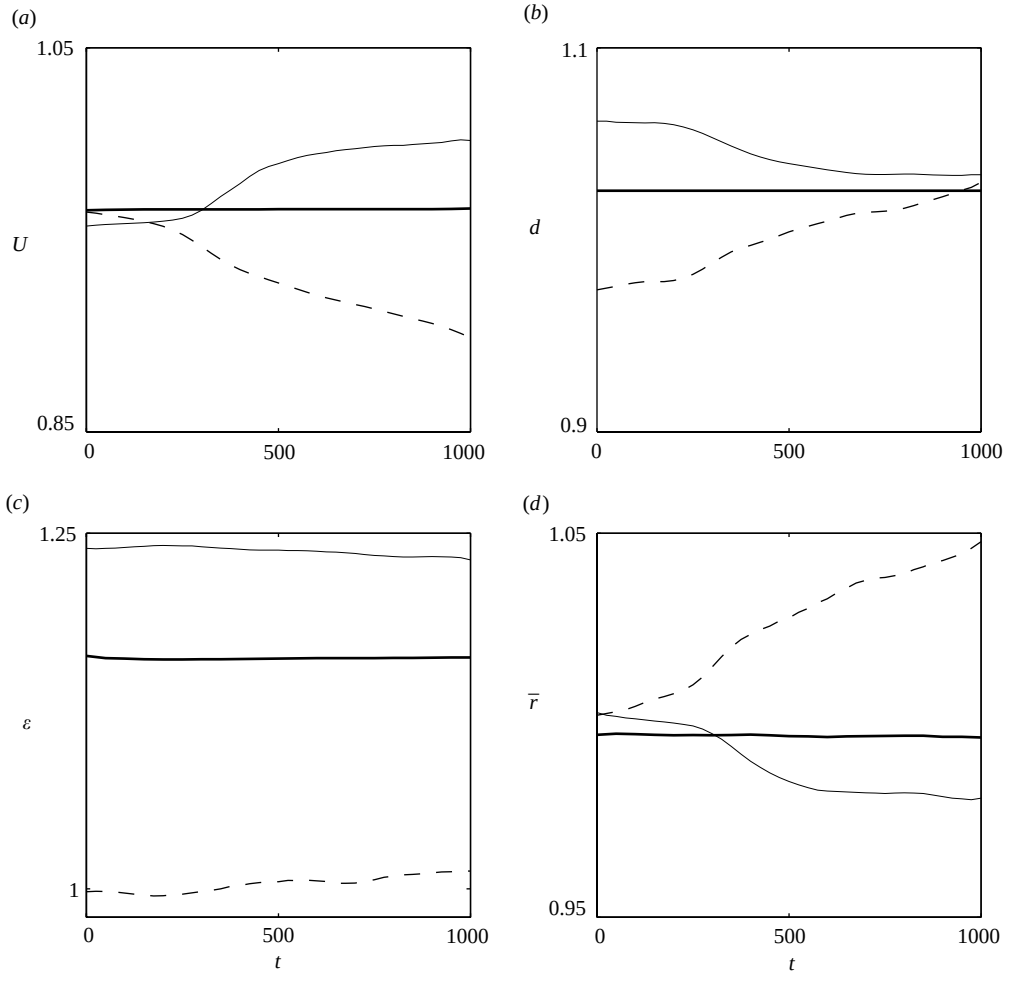

FIGURE 17. Evolution of parameters of the circular and ordinary elliptical f-plane modons with the nominal mean radius $\bar{r}=1$ and translation speed $U=1$: dashed line, the modon with the initial nominal aspect ratio $\varepsilon=1$; bold solid line, $\varepsilon=1.16$; thin solid line, $\varepsilon=1.25$; displayed parameters as in figure 13.

$300<t<500$ are the most significant: the mean radius decreases, the poles become closer and the translation speed grows (figure 17). At the last stage, from $t=500$ to $t=1000$, the vortex stabilizes and barely changes.

5. Conclusion

Using a combination of analytical and numerical methods (the approach suggested in Kizner *et al.* 2003), we have constructed and analysed a family of elliptical barotropic f- and β-plane dipole modons – both extended in the x-direction and those extended in the y-direction. Particular emphasis has been placed on the dependence between the conserved vorticity q and co-moving streamfunction Ψ in relation to the governing non-dimensional modon parameters. On the f-plane, there is only one such parameter, $\varepsilon=r_y/r_x$ – the aspect ratio characterizing the vortex form. On the

β-plane, translating modons are characterized by two parameters, ε and $\lambda^2 = \beta\bar{r}^2/U$, while a standing modon is determined by the form parameter ε only.

Strongly extended (in the x-direction) extraordinary modons on the β-plane were shown to have a typical dent in their q fields – a depression on a generally bell-like interior vorticity distribution – which is reflected by the upper end of the internal scattergraph being curved downwards and the lower end being curved upwards; on the f-plane, this was observed by Boyd & Ma (1990). Ordinary modons, i.e. those extended in the y-direction, do not have such a feature.

When the extension of an ellipse in the y-direction is sufficiently strong, the corresponding ordinary modon is shielded in terms of q. In such a modon, each of the dipole counterparts is encased in a band where q is of opposite sign (figure 5).

The most interesting finding is the existence of the so-called supersmooth modons. While in any non-shielded dipole on the β-plane there is always a jump of vorticity derivatives across the separatrix Γ, among the shielded β-plane modons for each λ^2 there exists a single supersmooth solution marked by the continuity of q derivatives at Γ; on the (λ^2, ε)-plane, such modons are represented by a continuous line that starts at the point $(0, \varepsilon_0)$ (see figure 1, line (iii)). In this point originates also the line that demarcates shielded modons from non-shielded modons (line (ii) in figure 1); it passes beneath the line of supersmooth solutions. On the f-plane, there is a unique supersmooth solution. It is just this solution that demarcates the pure and shielded modons; on the (λ^2, ε)-plane it is represented by the point $(0, \varepsilon_0)$. This solution is a limiting case (as $\lambda^2 \to 0$ and $\varepsilon \to \varepsilon_0$) of the β-plane elliptical modon solutions confined between lines (ii) and (iii) in figure 1.

Another limiting case (as $\lambda^2 \to \infty$) of an ordinary modon was also constructed (for mildly extended ellipses). This is the standing modon that exists only on the β-plane and necessarily has a vorticity jump across the vortex boundary.

Several numerical simulations of the evolution of elliptical modons were run to estimate and compare the stability properties of the elliptical solutions found. Two kinds of experiment were conducted: (i) using the base version of the model, where the perturbations are due to the finite size of the basin, periodical conditions at its western and eastern boundaries, finite-difference approximation and processor rounding off, and (ii) with periodical cutting of the peripheral vorticity, which in addition to the above listed perturbations hinders the modons in their eastward translation. Both ordinary ($\varepsilon \geqslant 1$) and extraordinary ($\varepsilon < 1$) solutions were tested. It was shown that dented extraordinary modons are clearly unstable and either disintegrate or evolve to the states with no dents. In contrast, non-dented configurations demonstrated a considerable resistance to small perturbations (both antisymmetric and asymmetric).

Our experiments point out that the supersmooth f- and β-plane solutions are stable, whereas the circular modons are presumably unstable, albeit rather durable. In the experiments with cutting, non-supersmooth non-dented modons demonstrate a tendency, in perspective, to gradually transform into supersmooth (though not strictly elliptical) states.

In geophysical applications, dipoles play a distinctive role, the apparent stability of the circular Lamb and Larichev–Reznik modons being one of the main reasons for their popularity. Taken together, our results signify that the forms of the observed vortices (or, alternatively, their q *vs.* Ψ relations) should be studied more thoroughly. Such a task looks feasible, at least, on a laboratory scale. Further, our numerical experiments with baroclinic modons (Kizner *et al.* 2002, 2003) indicate that, in stratified fluids, heton-like vortical structures represent a general type of equilibrium.

We believe, therefore, that an investigation of the stability or otherwise of barotropic modons to baroclinic perturbations might be of importance.

This research was supported by the Israel Science Foundation (Grant 616/00) and US–Israel Binational Science Foundation (BSF, Grant 2002392). Discussions with R. R. Trieling, V. Gryanik, G. Reznik, M. Sokolovsky, G. J. F. van Heijst and T. Smirnov where helpful. We are grateful to the anonymous referees whose comments led to improvements of the paper.

REFERENCES

Boyd, J. P. & Ma, H. 1990 Numerical study of elliptical modons using spectral methods. *J. Fluid Mech.* **221**, 597–611.

Brazier-Smith, P. R. 1984 On the limitations of spherical harmonics for the solution of Laplace's equation. *J. Comput. Phys.* **54**, 524–539.

Chaplygin, S. A. 1903 One case of vortex motion in fluid. *Trans. Phys. Sect. Imperial Moscow Soc. Friends Natural Sci.* **11**, N 2, 11–14 (in Russian).

Dritschel, D. G. 1988 Contour surgery – a topological reconnection scheme for extended integrations using contour dynamics. *J Comput. Phys.* **77**, 240–266.

Hesthaven, J. S., Lynov, J. P., Nielsen, A. H., Rassmussen, J. J., Schmidt, M. R., Shapiro, E. G. & Turitsyn, S. K. 1995 Dynamics of a nonlinear dipole vortex. *Phys. Fluids* **7**, 2220–2229.

Hesthaven, J. S., Lynov, J. P. & Nycander, J. 1993 Dynamics of nonstationary dipole vortices. *Phys. Fluids* A **5**, 622–629.

Kantorovich, L. V. 1948 Functional analysis and applied mathematics. *Yspekhi Matem. Nauk* N 3, 89–185 (in Russian).

Kizner, Z. & Berson, D. 2000 Emergence of modons from collapsing vortex structures on β-plane. *J. Mar. Res.* **58**, 375–403.

Kizner, Z. Berson, D. & Khvoles, R. 2002 Baroclinic modon equilibria on the beta-plane: stability and transitions. *J. Fluid Mech.* **468**, 239–270.

Kizner, Z. Berson, D. & Khvoles, R. 2003 Noncircular baroclinic beta-plane modons: constructing stationary solutions. *J. Fluid Mech.* **489**, 199–228.

Lamb, H. 1895 *Hydrodynamics* (2nd edn). Cambridge University Press.

Lamb, H. 1906 *Hydrodynamics* (3nd edn). Cambridge University Press.

Lamb, H. 1932 *Hydrodynamics* (6th edn). Cambridge University Press.

Larichev, V. D. & Reznik, G. M. 1976 Two-dimensional solitary Rossby waves. *Dokl. USSR. Acad. Sci.* **231**, 1077–1080.

Larichev, V. D. & Reznik, G. M. 1983 Colliding two-dimensional solitary Rossby waves. *Oceanologia* **23**, 725–734.

McWilliams, J. C. 1983 Interactions of isolated vortices. II: Modon generation by monopole collision. *Geophys. Astrophys. Fluid Dyn.* **19**, 207–227.

McWilliams, J. C., Flierl, G. R., Larichev, V. D. & Reznik, G. M. 1981 Numerical studies of barotropic modons. *Dyn. Atmos. Oceans* **5**, 219–238.

McWilliams, J. C. & Zabusky, N. J. 1982 Interactions of isolated vortices. I: Modons colliding with modons. *Geophys. Astrophys. Fluid Dyn.* **19**, 207–227.

Makino, M., Kamimura, T. & Taniuti, T. 1981 Dynamics of two-dimensional solitary vortices in a low-β plasma with convective motion. *J. Phys. Soc. Japan* **50**, 980–989.

Meleshko, V. V. & van Heijst, G. J. F. 1994 On Chaplygin's investigations of two-dimensional vortex structures in an inviscid fluid. *J. Fluid Mech.* **272**, 157–182.

Mezinger, F. & Arakawa, A. 1976 Numerical models used in atmospheric models. GARP Publication Series, **17**, 430.

McWilliams J. J. & Flierl, G. R. 1979 On the evolution of isolated, nonlinear vortices. *J. Phys. Oceanogr.* **9**, 1155–1182.

Morrel, Y. & McWilliams, J. 1997 Evolution of isolated interior vortices in the ocean. *J. Phys. Oceanogr.* **27**, 727–748.

Nielsen, A. H. & Juul Rasmussen, J. 1997 Formation and temporal evolution of the Lamb-dipole. *Phys. Fluids* **9**, 982–991.

Nycander, J. 1988 New stationary vortex solutions of the Hasegawa – Mima equation. *J. Plasma Phys.* **39**, 418–428.

Orlandi, P., Verzicco, R. & van Heijst, J. F. 1994 Stability of shielded vortex dipoles. In *Modelling of Oceanic Vortices* (ed. G. J. F. van Heijst), pp. 169–176. North-Holland.

Paldor, N. 1999 Linear instability of barotropic submesoscale coherent vortices observed on the ocean. *J. Phys. Oceanogr.* **29**, 1442–1452.

Stern, M. E. 1975 Minimal properties of planetary eddies. *J. Mar. Res.* **33**, 1–13.

Verkley, W. T. M. 1993 A numerical method to find form-preserving free solutions of the barotropic vorticity equation on a sphere. *J. Atmos. Sci.* **50**, 1488–1503.